Global and Planetary Change 185 (2020) 103096

Contents lists available at ScienceDirect

Global and Planetary Change

journal homepage: www.elsevier.com/locate/gloplacha

Research article

Climate and environmental response to the break-up of Pangea during the Early Jurassic (Hettangian-Pliensbachian); the Dorset coast (UK) revisited

Iris Schöllhorn[a,*], Thierry Adatte[a], Bas Van de Schootbrugge[b], Alexander Houben[c], Guillaume Charbonnier[a], Nico Janssen[c], Karl B. Föllmi[a,1]

[a] Institute of Earth Sciences, University of Lausanne, Géopolis, CH-1015 Lausanne, Switzerland
[b] Institute of Marine palynology and palaeoceanography, University of Utrecht, Princetonlaan 8a, 3584, CB, Utrecht, Netherlands
[c] Geological Survey of the Netherlands, TNO, Princetonlaan 6, 3584, CB, Utrecht, Netherlands

ARTICLE INFO

Keywords:
Early Jurassic
Climate change
Anoxia
Geochemistry
Break-up of Pangaea
Isotopes

ABSTRACT

Between the end-Triassic mass extinction and the Toarcian Oceanic Anoxic Event, the Early Jurassic witnessed important changes in carbon burial, palaeogeography and paleoceanography, which were linked to the initial breakup of Pangaea. In order to better understand the climate and environmental impact of this phase of major tectonic rearrangement we revisited a key section along the Dorset coast (UK) and used a multi-proxy geochemical approach for its analysis.

Carbon isotopes ($\delta^{13}C$) measured on organic matter were corrected for the influence of changes in the type of organic matter. The thus obtained $\delta^{13}C$-HI index and an additional $\delta^{13}C_{carb}$ record measured on bulk carbonate indicate a suite of carbon-isotope excursions (CIEs) including the negative main CIE (Triassic-Jurassic boundary to early Sinemurian) the negative Sinemurian-Pliensbachian boundary CIE and the positive *margaritatus* Zone (late Pliensbachian) CIE.

Based on elevated hydrogen index values and enrichments in Mo, U, V, total organic carbon (TOC) and pyrite, the Hettangian-Sinemurian interval was interpreted to have been characterised by high productivity conditions and strong oxygen depletion of the basin. The chemical alteration index (CIA), clay mineralogy, and $\delta^{18}O$ data provide independent evidence for increased continental runoff triggered by humid climate conditions on the adjacent continent during this time period. The strongest oxygen-depleted conditions were inferred for the lowermost Hettangian interval, coincident with the onset of the main negative CIE. A further less strongly oxygen-depleted interval was recorded through the negative CIE near the Sinemurian-Pliensbachian boundary (*jamesoni* and *ibex* Zones). This interval was characterised by drier conditions and possibly cooler water temperatures (e.g. CIA, $\delta^{18}O_{carb}$ and kaolinite/illite ratio).

Based on low CIA values and kaolinite/illite ratios, the Pliensbachian climate is considered to have been generally drier, superimposed by more humid episodes restricted to the *davoei* and *margaritatus* Zones. The long-term trend to drier conditions is explained by: (1) diminished atmospheric CO_2 contents due to a reduction in emissions of volcanogenic greenhouse gases, and/or; (2) changes in the palaeogeography and current patterns related to the break-up of Pangaea and more specifically to the opening of the Hispanic corridor.

1. Introduction

The Late Triassic – Early Jurassic interval is well known for two major environmental upheavals - the end-Triassic mass extinction event and the Toarcian Oceanic Anoxic Event (Hallam, 2002; Hesselbo et al., 2007; Ruhl et al., 2011; Van de Schootbrugge et al., 2013). However, an increasing number of studies highlight the fact that the intervening period (Hettangian-Pliensbachian) also witnessed important climate, environmental and oceanographic changes. This time interval is characterised by the breakup of Pangaea leading to the opening of the Hispanic Corridor during the latest Sinemurian-earliest Pliensbachian, and the less-well dated opening of the Viking strait (Aberhan, 2001; Van de Schootbrugge et al., 2005; Korte and Hesselbo, 2011). In addition, a series of important carbon-isotope shifts suggest major changes

* Corresponding author.
E-mail addresses: iris.91@hotmail.fr (I. Schöllhorn), thierry.adatte@unil.ch (T. Adatte), b.vanderschootbrugge@uu.nl (B. Van de Schootbrugge), alexander.houben@tno.nl (A. Houben), guillaume.charbonnier@unil.ch (G. Charbonnier), nico.janssen@tno.nl (N. Janssen), karl.foellmi@unil.ch (K.B. Föllmi).
[1] Deceased

https://doi.org/10.1016/j.gloplacha.2019.103096
Received 20 May 2019; Received in revised form 1 December 2019; Accepted 6 December 2019
Available online 12 December 2019
0921-8181/

in the carbon cycle, at least five of which appear to record global events. They correspond to the negative main carbon-isotope excursion (CIE) (earliest Jurassic), the negative Sinemurian-Pliensbachian boundary event, the late Pliensbachian positive CIE (*margaritatus* Zone), the end-Pliensbachian *spinatum* negative event and the Pliensbachian-Toarcian boundary event (Hesselbo et al., 2002; Suan et al., 2008, 2010; Ruhl et al., 2010; Porter et al., 2013; Bodin et al., 2016; Peti et al., 2016; Ruhl et al., 2016). The causes of these perturbations, their environmental and climatic impacts and their links with the aforementioned palaeogeographic changes are not yet well established.

The coastlines of southwestern England include reference sections for the Hettangian-Pliensbachian interval, which are amongst the best documented and well-dated archives for this time period (Lang et al., 1928; Cox, 1990; Hesselbo and Jenkyns, 1995, 1998; Page, 2010; Ruhl et al., 2016). We revisited the section of the Dorset coast and propose environmental and climate reconstructions for the Hettangian-Pliensbachian period, in order to better understand the impact of the changes in palaeogeography on the carbon cycle. Along the Dorset coast, around Lyme Regis and Charmouth, we sampled the interval spanning the Hettangian to the upper Pliensbachian (*margaritatus* Zone) and analysed the samples using a multi-proxy approach in order to reconstruct and trace: (i) links between sea-level change, mineralogical contents and sedimentation rates; (ii) carbon-cycle perturbations; (iii) marine oxygenation conditions and productivity, and; (iv) climate conditions.

1.1. Geographical location, geological context and sea-level change

The studied outcrop is located along the Dorset coast between Pinhay Bay and Eype Mouth, in southwest England. The lithological column, the ammonite zones and subzones and formations were provided by Lang et al. (1928), Cox (1990), Hesselbo and Jenkyns, 1995, 1998). The Triassic-Jurassic (T-J) boundary was placed following Page (2010) in comparison to the Hettangian GSSP in Austria at the base of the "Pre-planorbis" Beds of the basal Blue Lias Formation, at the base of the *tilmanni* zone, between the "initial" and "main" carbon isotopic excursions. The ages, ammonite zones and subzones and formations used for the study of the Dorset outcrop are represented in Fig. 1.

The measured and sampled succession has a total thickness of 292 m and covers the time interval between the base of the Hettangian and the late Pliensbachian (*margaritatus* Zone). Several hiatuses are present throughout the succession: a hiatus was invoked for the *angulata* Zone (Hettangian) on the basis of a regional correlation using Milankovitch cyclostratigraphy (Smith, 1989) and trends in clay mineral abundances (Deconinck et al., 2003). The origin of this hiatus was related to sea-level fall linked with the movement of one or more nearby faults (Radley, 2008). Major hiatuses were also recorded during the *denotatus* Subzone (*obtusum* Zone) and the entire *oxynotum* Zone and in the the *aplanatum* and *macdonnelli* Subzones (upper *raricostatum* Zone) (Hesselbo and Jenkyns, 1998; Deconinck et al., 2003; Hesselbo, 2008; Radley, 2008 and references therein). The origin of these hiatuses was explained by the combined effect of transgression-related sediment starvation, immediately followed by a prolonged period of regression (Hesselbo and Jenkyns, 1998). In addition, further hiatuses below conventional biostratigraphic resolution occur within the Blue Lias Formation (lithostratigraphic and magnetic-susceptibility analysis; uppermost Rhaetian to *bucklandi* Zone; Weedon et al., 2018), in the *luridum* Subzone (*ibex* Zone), in the *valdani* Subzone (strontium isotope data; *ibex* Zone; Jones et al., 1994) and in the *margaritatus* Zone (sedimentological features; Dyrham Formation; Hesselbo and Jenkyns, 1995 and cited references).

The Dorset section is located within the Wessex basin, in the centre of the Laurasian Seaway (Fig. 2). It is predominantly composed of hemipelagic mudstone with variable proportions of carbonate, marine organic matter (OM) and detrital materials, which becomes more sandy toward the top of the measured section (Fig. 3). This trend was interpreted as the result of a general regression (Hesselbo and Jenkyns, 1995; Warrington and Ivimey-Cook, 1995). Two members (Shales-with-Beef and Black Ven Marls) contain diagenetic limestone ("beef"; Marshall, 1982; Hesselbo and Jenkyns, 1995; Meng et al., 2017) that was formed by early overpressuring in organic-rich shales during burial.

Overall, sedimentation rates were lower during the Hettangian and the Sinemurian, and considerably enhanced from the mid-Pliensbachian onward. Relatively continuous, gradual deposition characterised both the Hettangian to early Sinemurian, as well as the early Pliensbachian, whereas deposition of asymmetric lithological cycles occurred during the late Sinemurian and late Pliensbachian (Hesselbo and Jenkyns, 1998; Weedon and Jenkyns, 1999).

In the British realm Early Jurassic sea-level change was studied and described in detail by Hesselbo and Jenkyns (1998), who reviewed previous studies and established and compared sea-level fluctuations in the Wessex, Cleveland, Hebrides and Bristol Channel Basins (Fig. 4). Maximum flooding surfaces were identified based on sediment starvation in distal areas and maximal accommodation in proximal areas. Conversely, sequence boundaries were equated with proximal erosion and bypass and maximal deposition in distal areas. The Dorset area of the Wessex Basin was considered to represent a distal setting from the Hettangian to at least the Early Pliensbachian (*ibex* Zone) (cf. Hesselbo and Jenkyns, 1998).

2. Material and methods

In total, 453 samples were collected at an average spacing of 65 cm. Several limestones were excluded as many are diagenetic in origin (mainly from the *semicostatum* to the *obtusum* Zones). A sample-related bias may therefore be considered. As the non-diagenetic limestones represents intervals of improved oxygenation conditions (Weedon and Jenkyns, 1999), which alternated with the oxygen-poor conditions, such conditions are poorly represented in this study. The geochemical and mineralogical analyses were all performed at the University of Lausanne (Switzerland).

Bulk-rock and clay mineralogy were analysed using a X-TRA Thermo-Arl SCINTAG 2000 diffractometer, following the procedures by Kübler (1983) and Adatte et al. (1996). The whole-rock mineralogy was determined by a semi quantitative method, using XRD peak intensities of the main minerals compared to external standards (Klug and Alexander, 1974; Kübler, 1983; Adatte et al., 1996) (Figs. 3 and 5). The precision corresponds to 5 wt% for grain minerals and 5 to 10 wt% for phyllosilicates. The clay mineralogy was determined on oriented slides of decarbonated samples and concentrated clay suspensions analysed by XRD (Adatte et al., 1996). Clay-mineral peak positions (2θ; Moore and Reynolds, 1989) were identified on diffractograms of ethylene-glycolated samples for the $< 2\,\mu m$ granulometric fraction. The intensities (in CPS) of the clay-mineral peaks were used for a semi-quantitative estimate of the proportion (in relative per cent) of clay minerals.

Sediment-accumulation rates were calculated for the Hettangian and the Pliensbachian for each ammonite zone using the time scale from Ruhl et al. (2010, 2016). Unfortunately, precise ages are not known for the Sinemurian ammonite zones and therefore the sedimentation rate was calculated for this entire stage using the durations from Ruhl et al. (2016). The durations of the hiatuses were calculated assuming equal length of the subzones and subtracted from the calculated total durations of the stages and ammonite zones. Sediment-accumulation rates for each component (X) were calculated using the following formula with X in wt%, the height in cm, the duration in Myr and 1.35 corresponding to the dry bulk density value for mudstone in g/cm^3 (Föllmi et al., 2005):

$$\text{Sediment} - \text{accumulation rates} = (X \times \text{Height} \times 1.35)/(100 \times \text{Duration}) \text{ (in g/cm}^2\text{/Myr)}$$

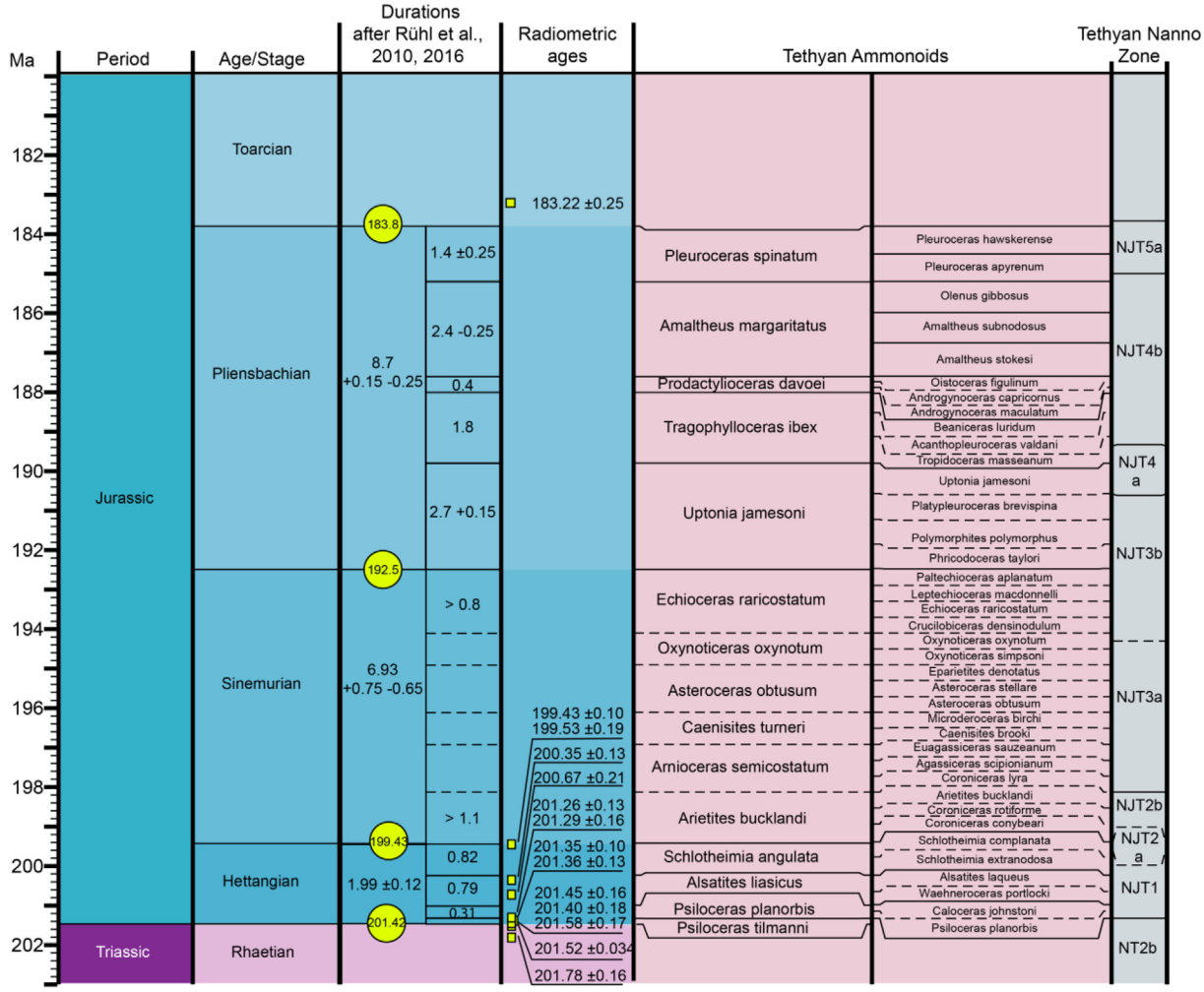

Fig. 1. Time scale, stages and Tethyan ammonite zones and subzones used for the Dorset section. The initial figure from Time Scale Creator was modified using the durations from Ruhl et al. (2010, 2016). The ammonite zones and subzones used for the English realm are from Hesselbo and Jenkyns (1998). Recently, a new duration was proposed for the Hettangian of ≥4.1 Myr. If used, the Sinemurian would be reduced in duration by around 2 Myr. The radiometric ages are from Kent and Olsen (2008), Schaltegger et al. (2008), Schoene et al. (2010), Guex et al. (2012a, 2012b), Blackburn et al. (2013), Hüsing et al. (2014) and Sell et al. (2014).

Preserved OM (273 samples) was analysed using a Rock-Eval 6 instrument following the methods described by Behar et al. (2001) and using standard IFP-160000 with an analytical error of < 0.1%. We measured total organic-carbon content (TOC), hydrogen index (HI), oxygen index (OI), thermal maturity (T_{max}) and mineral carbon content (MINC).

Oxygen and carbon-isotope analyses (402 samples) were performed using a Thermo Fisher Scientific GasBench II preparation device interfaced with a Thermo Fisher Scientific Delta Plus XL continuous flow isotope ratio mass spectrometer (IRMS). Data were calibrated to the

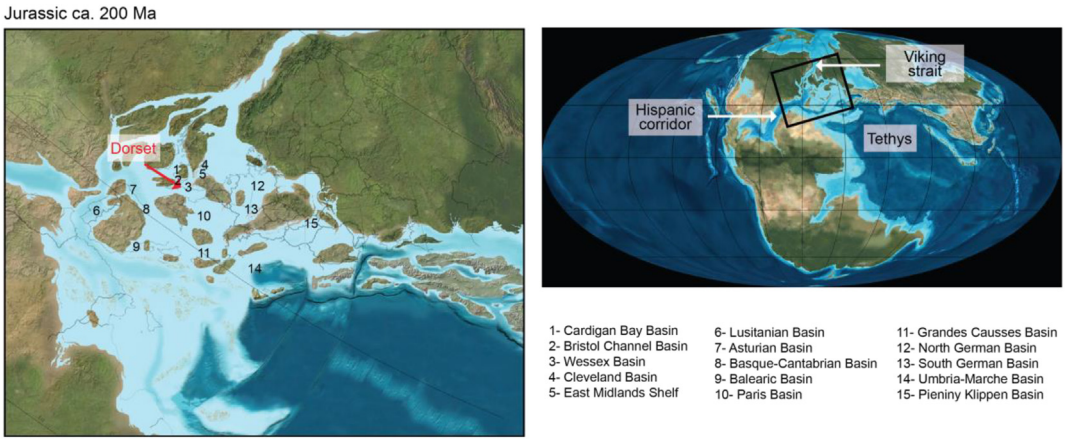

Fig. 2. Palaeogeographic reconstructions for the Early Jurassic. The world map is from Blakey (2014) and the European map from the website http://deeptimemaps.com/wp-content/uploads/2016/05/225_Trias_EurMap.png.

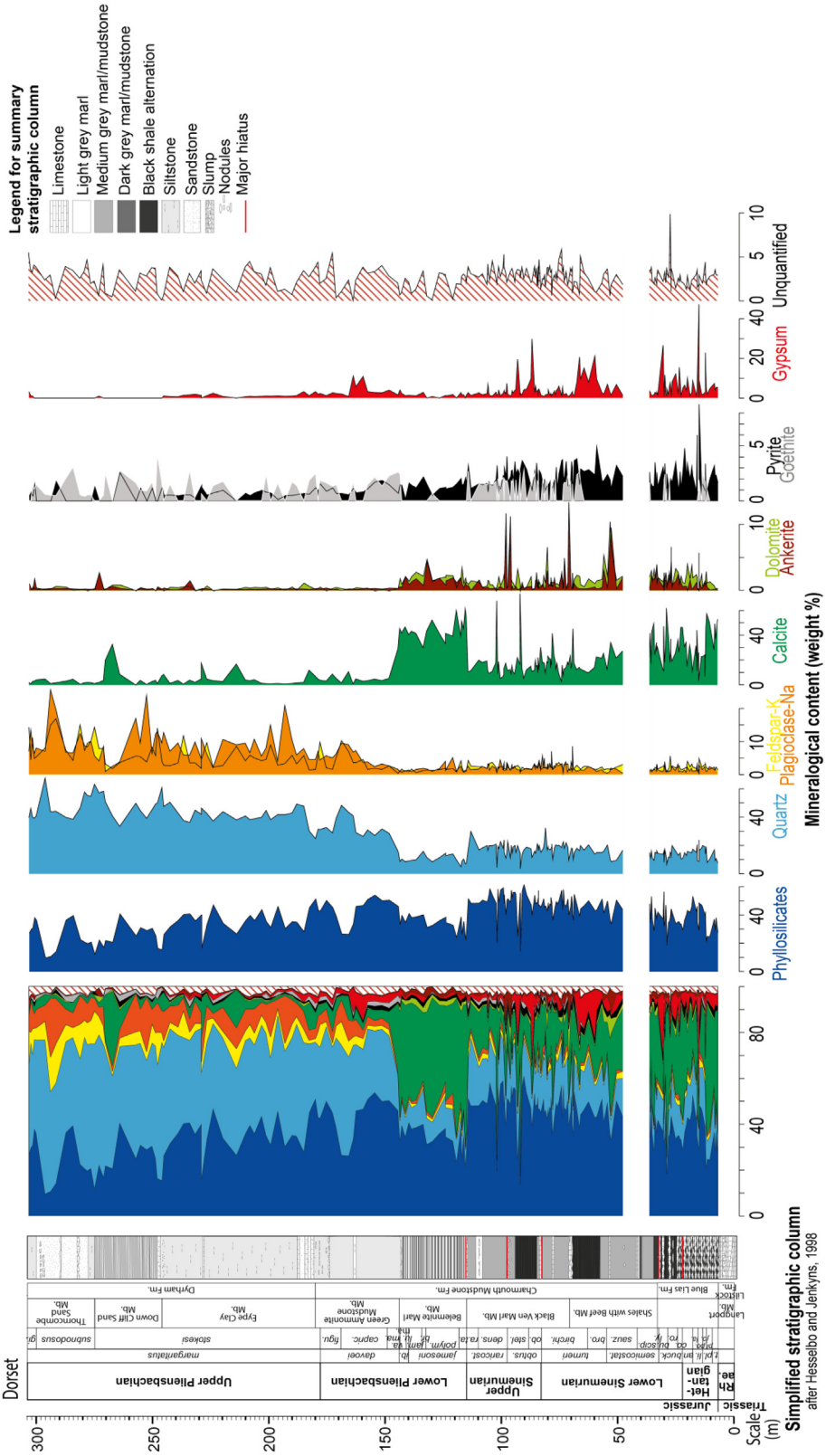

Fig. 3. Bulk mineralogical contents from the Dorset outcrop. The simplified stratigraphic column was modified after Hesselbo and Jenkyns (1998).

Vienna Pee Dee Belemnite scale (‰V-PDB). Analytical uncertainty (2σ) is not higher than ± 0.05‰ for $\delta^{13}C$ and ± 0.1‰ for $\delta^{18}O$.

The carbon-isotope composition of OM was analysed on decarbonated bulk sediment by flash combustion on a Carlo Erba 1108 elemental analyser connected to a Thermo Fisher Scientific Delta V isotope ratio mass spectrometer operating in continuous helium flow. The reproducibility, monitored by standard measurements, is better than 0.1‰ (1σ).

Changes in the OM type may induce shifts in the $\delta^{13}C_{org}$ record of up to 2–4‰ (e.g., Toarcian Oceanic Anoxic Event; Suan et al., 2015). In

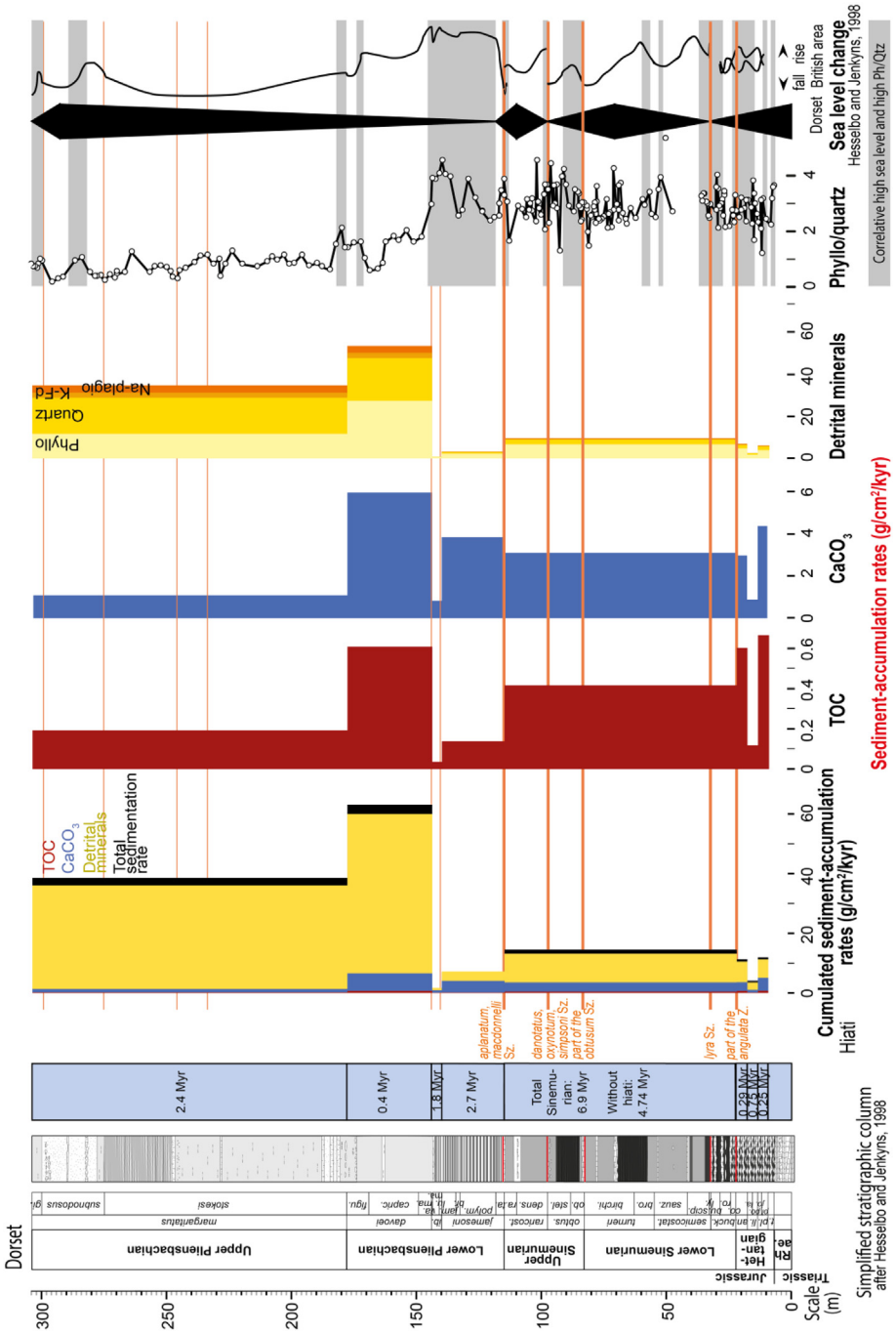

Fig. 4. Calculated sedimentation rates for TOC (total organic content), $CaCO_3$ (carbonate) and detrital mineral contents from Dorset. Rates were calculated based on the durations for stage and ammonite zones proposed by Ruhl et al. (2010, 2016). The phyllosilicate/quartz ratio is compared to sea-level change from the English realm reconstructed by Hesselbo and Jenkyns (1998).

the Dorset section, HI values fluctuate between 32 and 710 mg HC/g TOC indicating strong changes within the OM type. Therefore, in order to remove the effect of the OM type on the carbon isotopes we made a correction based on the HI values using the methodology developed by Van de Schootbrugge et al. (2013) and Suan et al. (2015). The calculations are based on the following formula:

$$\delta^{13}C - \text{HI index} = \delta^{13}C_{org}\ \text{measured} - (a \times HI)$$

The obtained curve, called δ^{13}C-HI index, allows visualisation of the changes in the $\delta^{13}C_{org}$ data, that are not related to changes in the type and source of organic matter (OM). For this method the first step used here was to determine the precise relation between HI and $\delta^{13}C_{org}$ records. This is deduced from the equation obtained from the linear correlation between HI and $\delta^{13}C_{org}$ values from samples in intervals lacking exogenic carbon-isotope excursions. In our case this is rather difficult because it is not clear where such excursions precisely start and end. We therefore established different curves for several parts of the $\delta^{13}C_{org}$ record not involved in steep isotope shifts (Fig. 6). The curves present similar slopes (a). The obtained δ^{13}C-HI index curves were drawn for all slopes characterised by high R^2 ($0.51 < R^2 < 0.80$) with the exception for one that records a different a value ($a = -0.0034$). The four considered equations present a similar a factor ($a = -0.0092$; $a = -0.0064$; $a = -0.0079$; $a = -0.0083$) (Fig. 6). This similarity indicates a good reliability for the approach used here. The low R^2 from

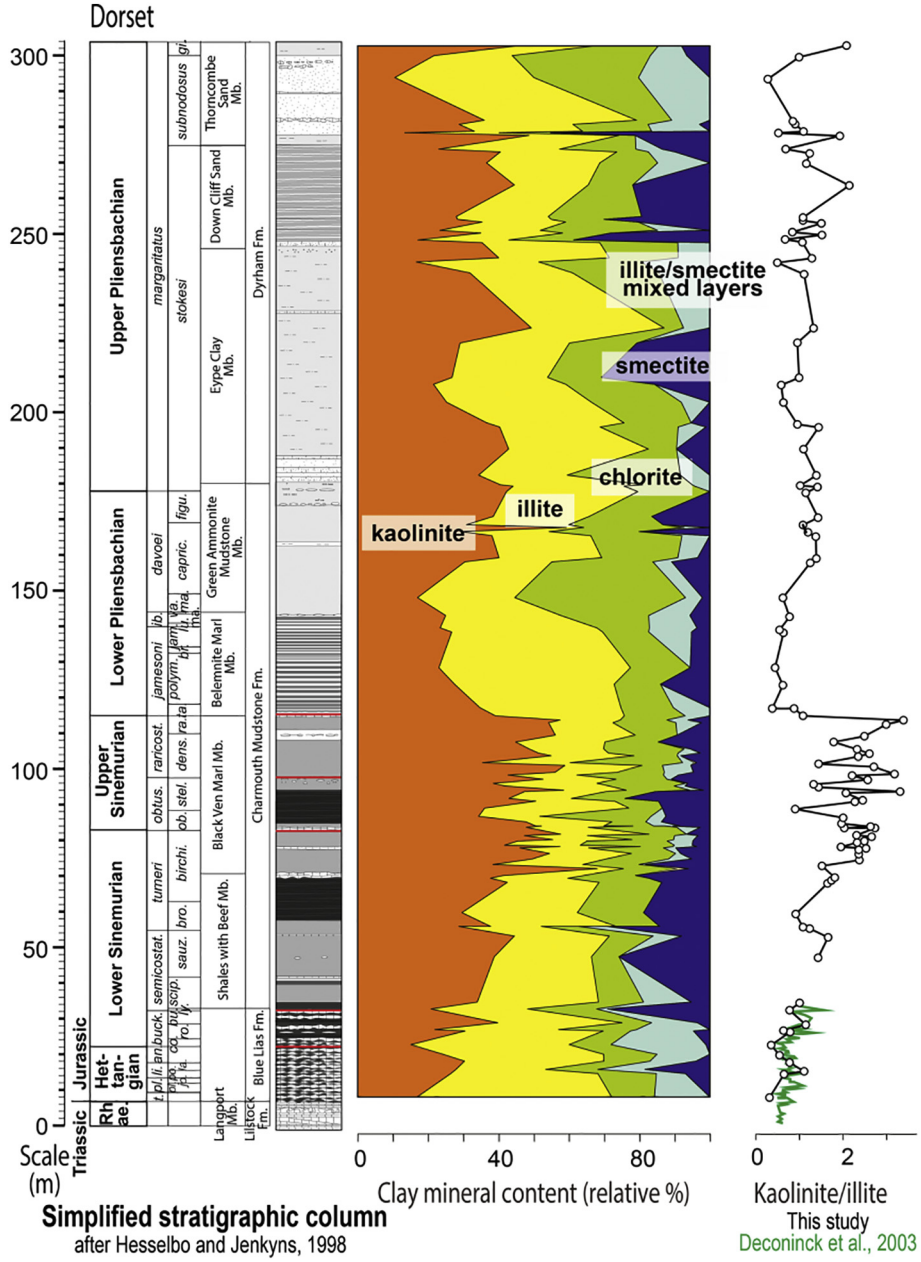

Fig. 5. Clay mineralogy and kaolinite/illite ratios from the Dorset outcrop.

the other parts of the sections are probably explained by the consistently low range of the HI index in those parts.

Major- and trace-element (ME and TE) concentrations were determined by X-ray fluorescence spectrometry (120 samples), using a spectrometer XRF Philips PW2400 with Rh-Kα radiations and a power of 2400 W. The detection limits are approximately 0.01% for MEs and 1 to 7 ppm for TEs. The external reproducibility (1σ) varies between 0.5 and 5% depending on the element. The accuracy of these analyses was assessed by the analysis of standard reference materials (NIM-G; SDC; BHVO; QLO).

The chemical index of alteration corrected for carbonate with and without K_2O (CIA*-K and CIA*) was calculated to characterize precipitation rates on the adjacent land (Nesbitt and Young, 1982, 1989; Fedo et al., 1995; Yan et al., 2010). The index reflects the decomposition of unstable minerals (plagioclase) into clays. For this study, one correction was made (Nesbitt and Young, 1982, 1989). The CaO values (Formula 1) were replaced by Na_2O (Formula 2) because the contents of CaO in the Dorset sections vary as a function of environmental conditions (redox and sea-level change) and diagenetic processes. Certain limestone beds are linked to diagenesis (Marshall, 1982; Hesselbo and Jenkyns, 1995; Meng et al., 2017). Formula 2 was calculated with and without K_2O in order to test the effect of illitisation processes. The two curves show the same trends. This in addition with the clay-mineralogical composition shows that illitisation processes have not affected the CIA trends and therefore formula (2) can be used.

$$CIA = Al_2O_3 \times 100/(Al_2O_3 + CaO + Na_2O + K_2O) \text{ (in molar proportion)} \quad (1)$$

$$CIA = Al_2O_3 \times 100/(Al_2O_3 + 2 \times Na_2O + K_2O) \text{ (in molar proportion)} \quad (2)$$

The enrichment factor of trace elements (TEs) relevant for the reconstruction of palaeo-redox conditions was calculated using the following formula (Wedepohl, 1971, 1991; McLennan, 2001).

$$X_{EF} = (X/Al)_{sample}/(X/Al)_{standard} \text{ (in ppm proportion)}$$

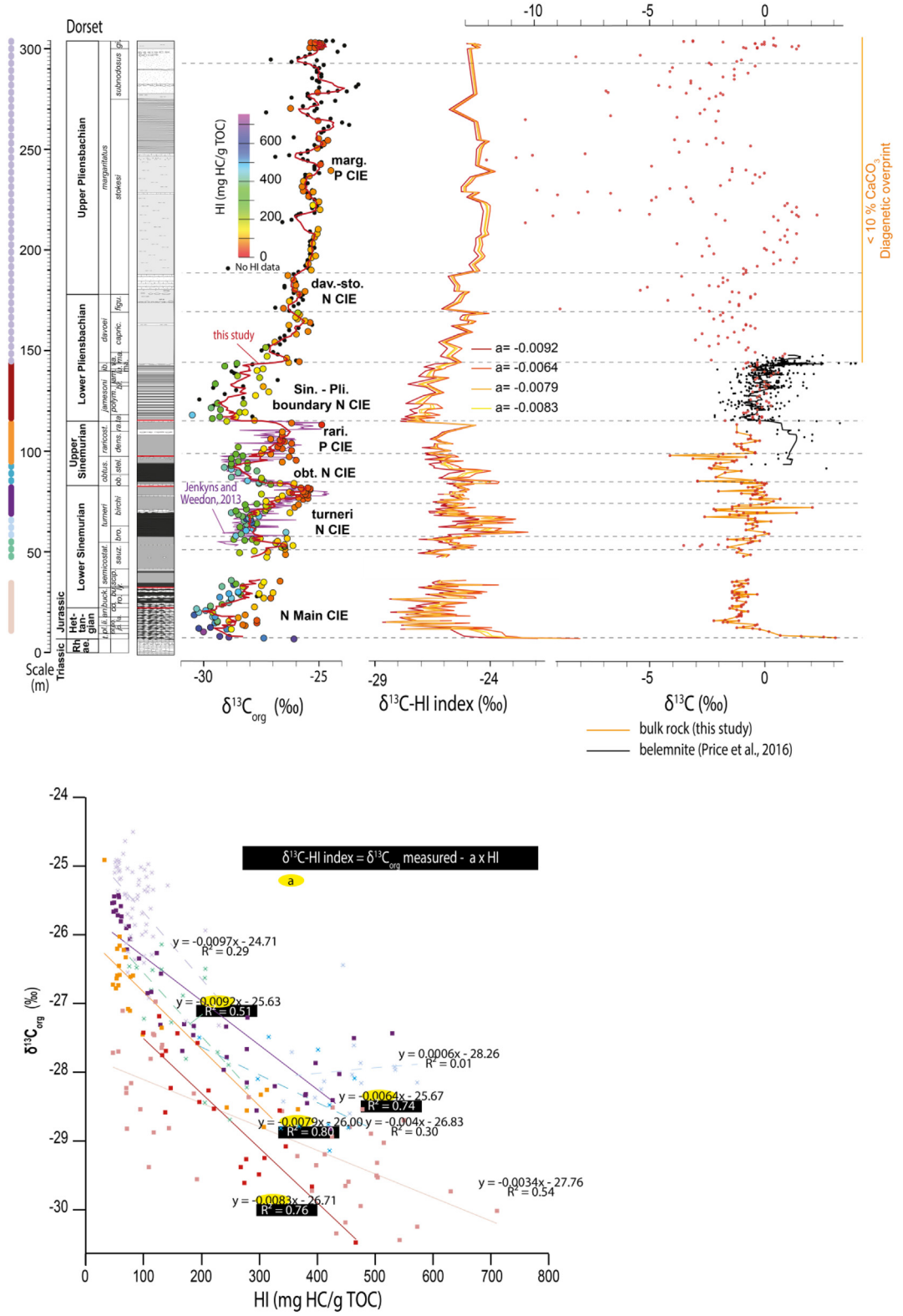

Fig. 6. Stratigraphic variations of the measured and corrected organic-carbon isotopes ($\delta^{13}C_{org}$ and δ^{13}C-HI index), and carbon isotopes measured on bulk carbonate ($\delta^{13}C_{carb}$) along the Dorset section. The δ^{13}C-HI index is based on the best-fitting correlation between the $\delta^{13}C_{org}$ and HI data shown below. P means positive and N negative.

Post-Archaean average shale (PAAS) is used as the standard to evaluate relative enrichment/depletion with the exception of Mo, which is normalised by using North American shale composite (NASC) as a standard because Mo was not measured in PAAS (Wedepohl, 1971; Anders and Grevesse, 1989). To supplement the information on palaeo-oxygenation conditions, the ratios of combined TEs, such as Mo vs V/Mo and Mo_{EF} vs. U_{EF} were also analysed (Algeo and Tribovillard, 2009; Piper and Calvert, 2009).

3. Results

3.1. Mineralogy

3.1.1. Bulk-rock mineralogy

The mineralogy of the Dorset section is mainly composed of quartz, phyllosilicates, K-feldspar, Na-plagioclase and calcite, with lower proportions of dolomite, ankerite, pyrite, goethite and gypsum (Fig. 3). The unquantified fraction includes mainly poorly crystallised phyllosilicates, Fe-oxides and –hydroxides and other minerals, in addition to organic matter. Following the mineralogical content, the section can be divided into three parts.

The first part, spanning the Hettangian and the Sinemurian interval (7 to 115 m), is characterised by a clayey composition. It consists of 44.5 wt% phyllosilicates, 21 wt% calcite and 16 wt% quartz, with lower proportions of gypsum (5 wt%), unquantified material (3 wt%) and small amounts of K-feldspar, Na-plagioclase, dolomite and pyrite (2 wt % in total) (Fig. 3).

The second part, covering the *jamesoni* and *ibex* Zones (lowermost Pliensbachian, 115 to 143.9 m), contains more carbonate with an average of 45 wt% calcite associated with 33.5 wt% phyllosilicates, 10 wt% quartz and low amounts of Na-plagioclase, dolomite and an unquantified fraction (2 wt% in total). In addition, K-feldspar, pyrite, gypsum and ankerite are present but in proportions lower than 1.5 wt% (Fig. 3).

The last part covers the *davoei* and *margaritatus* zones (upper lower Pliensbachian to the lower upper Pliensbachian; 143.9 to 303 m) and is dominated by detrital minerals, with 42 wt% quartz and 33 wt% phyllosilicates on average. The remaining fraction is composed of 8 wt% Na-plagioclase, 6 wt% K-feldspar and calcite, 3 wt% unquantified material and < 1.5 wt% dolomite, pyrite, goethite, gypsum and ankerite (Fig. 3).

3.1.2. Clay mineralogy

Clay mineral assemblages consist mainly of kaolinite, illite, chlorite, irregular R0 type illite/smectite mixed-layer (referred to smectite in the following sections and Fig. 5) and R1 type illite/smectite mixed-layer (referred to illite/smectite mixed layer in the following sections and Fig. 5) and record large-scale stratigraphic variations (Fig. 5).

From the base of the section to the Sinemurian-Pliensbachian boundary (7 to 115 m) the kaolinite/illite ratio (K/I) increases from 0.8 to 2. This general trend is modulated by several lower amplitude oscillations, which occurred through the Sinemurian. At the Sinemurian-Pliensbachian boundary (115 m) the K/I ratio drops abruptly to values of around 0.9. In the *davoei* Zone (upper lower Pliensbachian, 144 m) K/I values increase again, reaching around 1.8 and remain between 1 and 2 to the top with two highs observed at the top of the *stokesi* Zone and in the *gibbosus* Zone (upper Pliensbachian).

3.2. Isotope geochemistry

3.2.1. $\delta^{13}C_{org}$

$\delta^{13}C_{org}$ values range from −30.5 to −23.3‰ and record several significant positive and negative shifts (Fig. 6). At the Triassic-Jurassic boundary (at 7 m) the $\delta^{13}C_{org}$ data show an abrupt shift of −4‰. Then, they increase gradually by 4‰ reaching the highest values in the *semicostatum* Zone (lower Sinemurian). Above, a second abrupt negative shift of 2‰ is recorded at 55 m, and in the following, the record remains stable until the upper *turneri* Zone (lower Sinemurian, 69 m). At this point the values start to increase by 3‰ up to the top of the *turneri* Zone (83 m). A negative shift of 3.3‰ characterises the *obtusum* Zone (83–97 m). The *raricostatum* Zone (83–115 m) shows a positive shift of 2.5‰, which is followed by an important and steep negative shift of 5‰ at the Sinemurian-Pliensbachian boundary (115 m). Then, from the top of the *ibex* Zone to the *davoei* Zone the $\delta^{13}C_{org}$ record returns to values of around 25.5‰ (144 m). Above, the $\delta^{13}C_{org}$ record remains stable with the exception of a few negative spikes of around 1‰ recorded in the upper Pliensbachian and a positive shift in the *subnodosus* Zone (281 m) (Fig. 6).

The δ^{13}C-HI index preserves the general trends with negative CIEs recorded during the Hettangian – lowermost Sinemurian (*bucklandi-semicostatum* Zones), in the *obtusum* Zone and at the Sinemurian-Pliensbachian boundary (*jamesoni* and *ibex* Zones) (Fig. 6). The *margaritatus* Zone (upper Pliensbachian) preserved the most positive $\delta^{13}C$ values of the section. However, the *turneri* negative CIE (−2‰) disappeared almost entirely following the correction, and the *obtusum* and the Sinemurian-Pliensbachian boundary negative CIE's are both diminished (from −3.5 to −2‰, and − 4 to −2‰, respectively).

3.2.2. $\delta^{13}C_{carb}$

From the base to 110 m in the section the $\delta^{13}C_{carb}$ values range from −2.4 to 3.1‰, with the exception of some outlier data (Fig. 6). They record shifts similar to the $\delta^{13}C_{org}$ ones but with different amplitudes. Right below the Triassic-Jurassic boundary (at 7 m) the $\delta^{13}C_{carb}$ shows an abrupt shift of 5‰. Then, the values increase gradually by 1.5‰ reaching the highest values in the *semicostatum* Zone (lower Sinemurian). At around 64 m, a second abrupt negative shift of 1.7‰ is recorded and above, values increase by 2.2‰ in the *turneri* Zone (lower Sinemurian, 73 m). A negative shift of 4‰ characterises the *obtusum* Zone (83–97 m). Right above, a positive shift of 3‰ is observed and the values remain high and stable until the top of the *ibex* Zone (lower Pliensbachian, 150 m).

In the interval from the *davoei* to the *margaritatus* Zones, $\delta^{13}C_{carb}$ analyses were performed but the very low average $CaCO_3$ contents (around 4%) appear to have completely offset the values. $\delta^{13}C_{carb}$ data comprise values between −12.1 and 2.3‰ and the widespread of data in the interval precludes their use in any palaeoceanographic or palaeoenvironmental reconstruction (Fig. 6).

3.2.3. $\delta^{18}O_{carb}$

The oxygen-isotope record shows an abrupt negative shift of 2.8‰ right below the Triassic-Jurassic boundary (at 7 m, Fig. 7). Above the boundary, the record is characterised by several positive and negative shifts. Following the Sinemurian-Pliensbachian boundary, at 115 m (*jamesoni* and *ibex* Zones,) a positive trend shifts the data to around 1.5‰.

3.3. Organic matter characterisation

From the base of the Hettangian to the lowermost Pliensbachian (7 to 144 m), the total organic carbon (TOC) content and HI are fluctuating between very high (up to 13 wt% TOC and 710 mg HC/g TOC HI values) and low values (down to 0.5 wt% TOC and 32 mg HC/g TOC HI values) (Fig. 8). From 144 m up to the top of the section (Pliensbachian), the TOC and HI values remain low with no significant trends ($TOC_{average}$ = 0.6 wt% and $HI_{average}$ = 79 mg HC/g TOC) (Fig. 8). The T_{max} record presents relatively constant values ranging around 422 °C with a standard deviation of 13 °C (Fig. S1; supplementary files). This demonstrates that the organic matter is immature and that there was a weak thermal diagenetic overprint (Espitalie et al., 1986).

From the base up to the mid *margaritatus* Zone (upper Pliensbachian, 7 to 260 m) the OI values are quite low and fluctuate around 50 mg CO_2/g TOC. The upper 43 m (the upper part of the *margaritatus* Zone; upper Pliensbachian, 260 to 303 m) are characterised by a high OI of around 255 mg CO_2/g TOC. This interval correlates with the deposition of coarse silty grainstone with low organic matter content.

3.4. Redox sensitive trace elements (RSTEs)

The TEs considered here are vanadium (V), molybdenum (Mo), uranium (U), nickel (Ni) and copper (Cu) (Figs. 8 and 9). From the base to the lowermost Pliensbachian (7 to 145 m) the section shows an

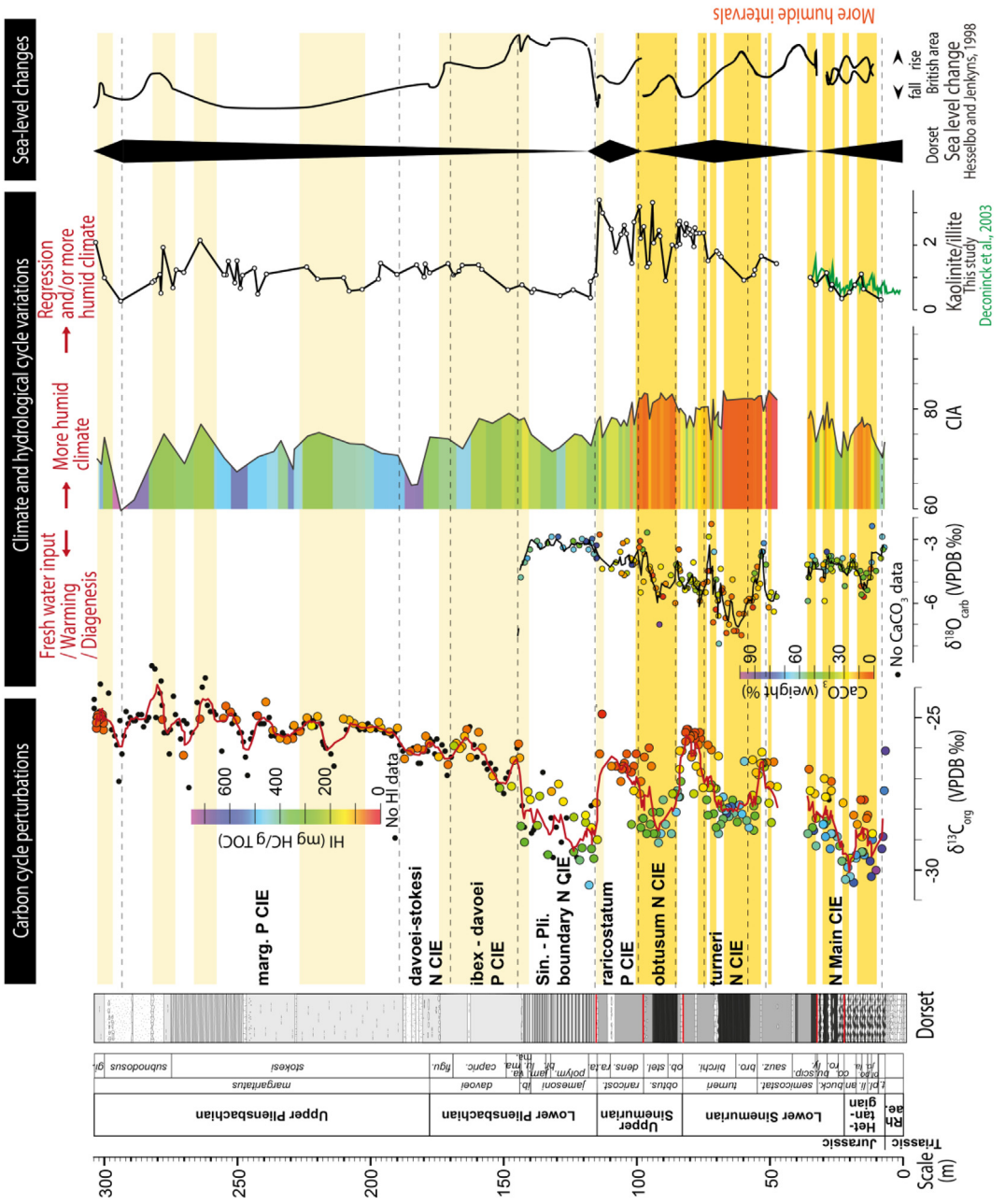

Fig. 7. Proxies of climate and the hydrological cycle compared to the carbon-isotope record and sea-level change along the Dorset section (δ^{13}C-HI index; $\delta^{13}C_{carb}$; $\delta^{18}O_{carb}$ of bulk carbonate and belemnites (Price et al., 2016); chemical index of alteration (CIA); kaolinite/illite ratios (partly from Deconinck et al., 2003), and magnetic susceptibility (Deconinck et al., 2003). P means positive and N negative.

alternation of intervals that are enriched in these trace elements with intervals that have values close to average shale (Post-Archean average shale; PAAS; and North American shale composite; NASC). The enriched intervals are located at the base of the section (Hettangian-lower Sinemurian), within the lower Sinemurian *turneri* Zone, in the lower upper Sinemurian and in the lowermost Pliensbachian (Fig. 8). The enriched layers record enrichment factors (EFs) going up to $EF_{Mo} = 127$, $EF_U = 7$ and $EF_V = 3$. Above 145 m (upper lower Pliensbachian) the values remain low with no further major increase up to the top of the section.

3.5. Chemical Index of Alteration (CIA)

The CIA records values between 59 and 84 (Fig. 7). The index shows an increase right above the Triassic-Jurassic boundary and remains high with the exception of small-scale variations up to the upper Sinemurian (96 m). The CIA decreases from the *raricostatum* Zone up to the *davoei* Zone (103–144 m). Within this latter zone, the index shows increasing values again. Further up to the top of the section (144 to 303 m) the samples are characterised by generally decreasing values, superimposed by three smaller amplitude shifts (Fig. 7).

4. Discussion

4.1. Detrital input, sedimentation rates and sea-level change

XRD analyses were performed on the Dorset section in order to understand the link between the stratigraphic evolution of the mineralogical composition, sea-level change and climate variations. The sediments of the studied section are predominantly composed of detrital

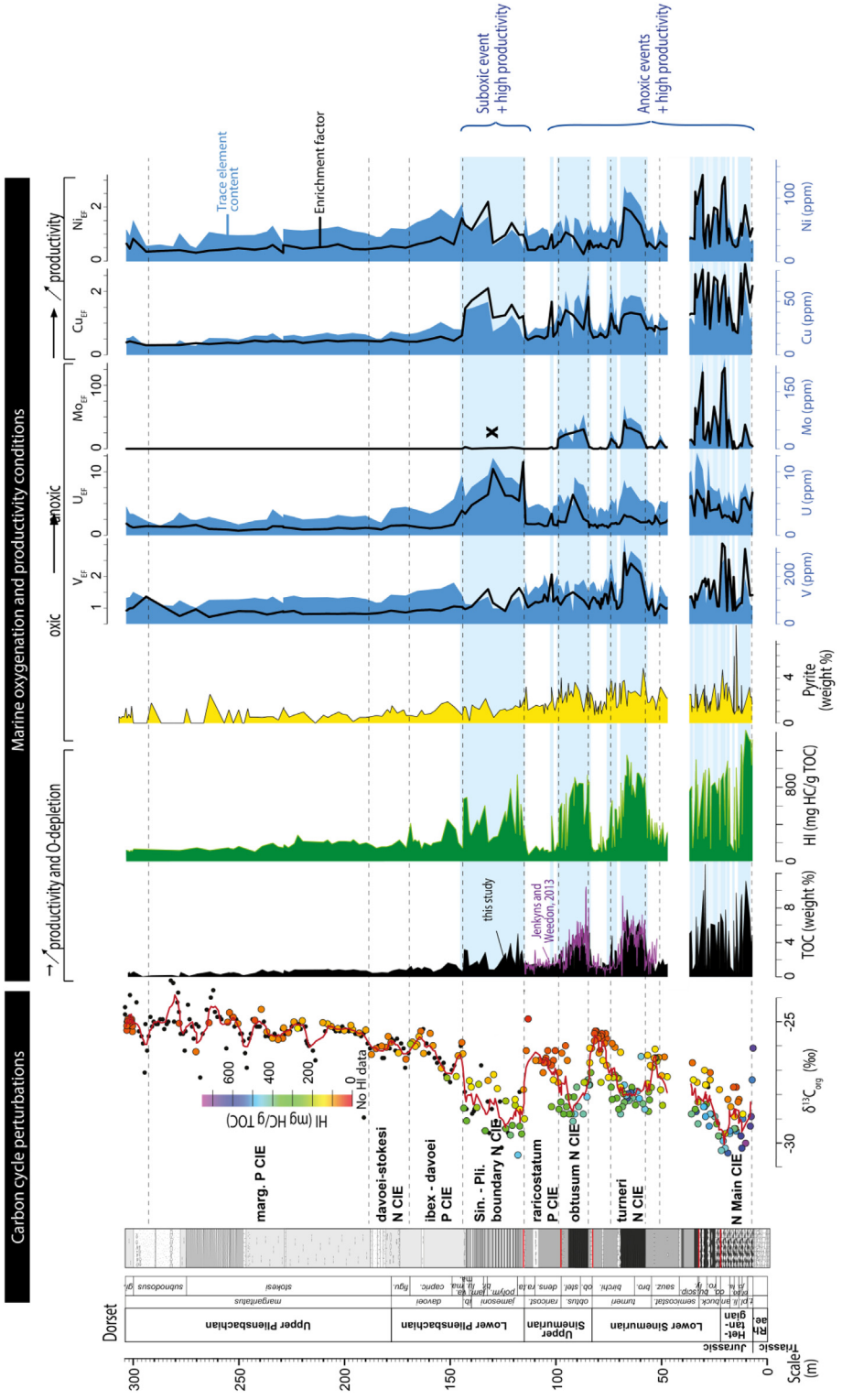

Fig. 8. Marine oxygenation and productivity conditions compared to carbon-isotope changes. Reconstructions of oxygenation and productivity variations are based on total organic carbon (TOC) content, hydrogen index (HI) and pyrite content, in addition to vanadium (V), uranium (U), molybdenum (Mo), copper (Co) and nickel (Ni) contents and enrichment factors (EF). P means positive and N negative.

minerals (quartz, K-feldspar, Na-plagioclase; Fig. 3). Temporal variations in their accumulation largely controlled overall changes in sediment-accumulation rates, as is shown by the calculated sediment-accumulation rates of different mineral components (Fig. 4).

Changes in the relative amount of quartz and phyllosilicates within the detrital materials were mainly influenced by sea-level change as is suggested by the good correlation between the phyllosilicates:quartz (Ph/Qtz) ratio and the sea-level interpretation of Hesselbo and Jenkyns (1998) (Fig. 4). This is likely related to the differential settling characteristics of these two mineral groups, with higher Ph/Qtz values recorded during higher sea level and vice versa. The Hettangian and Sinemurian stages are characterised by relatively high sea level, and the

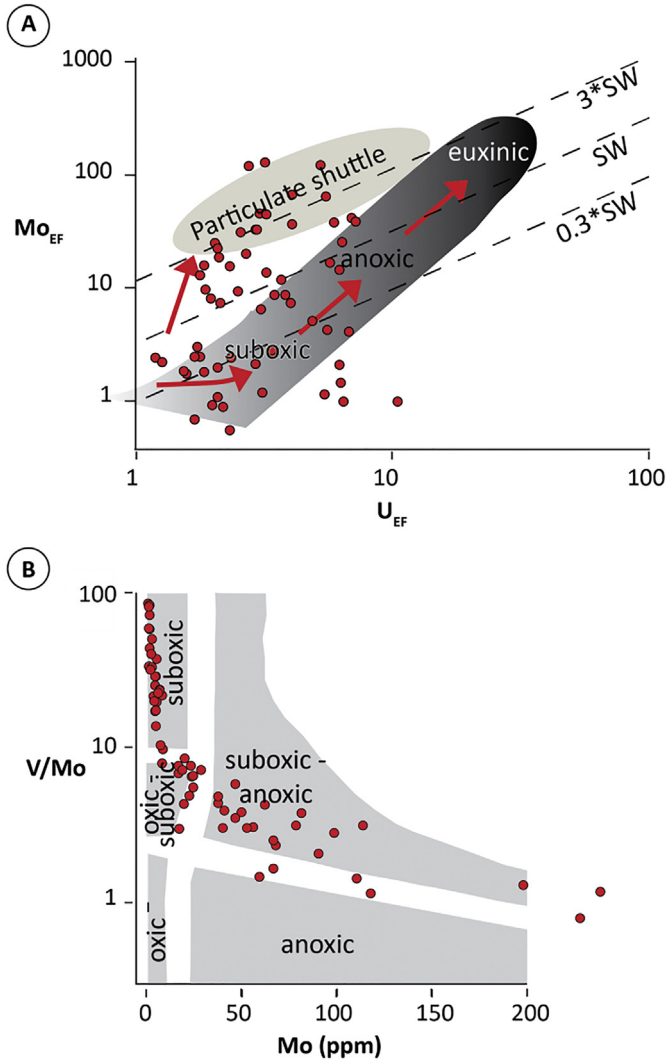

Fig. 9. Marine oxygenation conditions based on (A) Mo and U enrichment factors (EF) (Algeo and Tribovillard, 2009) and (B) (V/Mo) ratio vs. Mo (Piper and Calvert, 2009).

corresponding sediments show a more clayey composition with a high Ph/Qtz ratio (2.9; Fig. 4). Above the Sinemurian-Pliensbachian boundary, an increase in the ratio (3.5) is observed, which is the likely consequence of a deepening environment (Hesselbo and Jenkyns, 1998). Subsequently, up to the top of the *margaritatus* Zone, a decrease (0.9) is detected, which can be linked with a phase of sea-level fall (Hesselbo and Jenkyns, 1998). Smaller increases are observed in the *davoei* and *subnodosus* Zones (upper *margaritatus* Zone), which are superimposed on the long-term decrease.

An exception might be provided by the interval of the *davoei* Zone (lower Pliensbachian), which shows the highest sediment-accumulation rates. According to Hesselbo and Jenkyns (1998), this period would correspond to an intermediate regressive phase (Fig. 4). Based on Nd isotopes, $\delta^{18}O$ of fish tooth, clay-mineral analyses and a numerical model (the Fast Ocean–atmosphere Model), Dera et al. (2009a, 2009b, 2015) and Dera and Donnadieu (2012) demonstrated that in the Euro-boreal region a warming phase occurred during the *davoei*-lowermost *margaritatus* Zones, which may have been linked with an incursion of warm Tethyan waters. This warming trend is confirmed by palaeo-phytogeographic analyses (Rees et al., 2000) and oxygen isotope data measured on bulk rock and belemnites (Bailey et al., 2003; Arabas et al., 2017). Propitious climate and palaeoceanographic conditions may therefore have favoured the increased input of sediment and in particularly of phyllosilicates into this basin during this time period. As all mineral components record increased accumulation rates during the *davoei* Zone, it is not excluded that an underestimation of the length of time involved in this biozone may have artificially increased the calculated rates. Indeed, it is likely that the deposition of sediments dated from the *margaritatus* Zone was highly episodic and with correspondingly higher sedimentation rates than inferred for the deposited sediments.

The long-term sediment-accumulation rate of $CaCO_3$ is rather small relative to the overall sediment-accumulation rates and likely not sufficient to impact these rates. Even in the interval corresponding to the lower Pliensbachian (*jamesoni* Zone), which is characterised by the highest carbonate content (56 wt% $CaCO_3$), the high $CaCO_3$ content appears to have mainly been caused by lower detrital dilution related to high sea level (Hesselbo and Jenkyns, 1998) rather than by changes in carbonate production rate (Fig. 4). Furthermore, the vertical migration of carbonate during diagenesis may have affected the sediment-accumulation rates for $CaCO_3$ calculated for the Hettangian-Sinemurian interval. Organic matter (OM) and other components are not present in sufficient quantities to have significantly impacted overall sediment-accumulation rates as well.

In general, in the Dorset section, the Hettangian and Sinemurian intervals are characterised by lower sediment-accumulation rates in comparison to the Pliensbachian interval. This general trend correlates rather well with the regressive trend inferred for the Early Jurassic (Hesselbo and Jenkyns, 1998; Haq, 2017; Fig. 4).

It should also be noted that the sediment-accumulation rates are based on the durations calculated by Ruhl et al. (2010, 2016). Recently, Weedon et al. (2018) proposed a duration for the Hettangian stage, which is twice as long as the one previously proposed, coupled with a Sinemurian stage, which would be around 2 Myr shorter. This would divide the calculated sediment-acculumation rates of the Hettangian by two and the sedimentation rate for the Sinemurian interval would rise by around 30%. In addition, the presence of further hiatuses below conventional biostratigraphic resolution (e.g., chapter 5.1.) may partly have modified the calculated sediment-accumulation rates.

4.2. Carbon isotope records

In order to obtain better insight into changes in the carbon cycle and compare them to earlier records and records from other basins, we produced a high-resolution long-term isotope record both from bulk organic matter (OM), as well as from bulk carbonate (Fig. 6). Given the highly variable HI values through the first 180 m of the Dorset section (up to the lower to upper Pliensbachian boundary interval), we corrected the carbon-isotope data obtained on OM for the influence of changes in OM type and source (cf. section material and methods). In our case these methodology appears to be valid because of the good correlation between the $\delta^{13}C_{org}$ and HI data (Fig. 6; $0.51 < R^2 < 0.80$) in those intervals, which are not involved in pronounced isotope shifts related to changes within the general carbon cycle.

HI values may also be artificially decreased by changes in the quality and quantity of calcium carbonate and clay minerals, in addition to diagenetic processes (Espitalié et al., 1984; Spiro, 1991). We lack evidence that diagenesis considerably affected HI values, as the burial depth did not exceed 1 km (Deconinck et al., 2003) and as the T_{max} values are mostly between 409 and 435 °C (Fig. S1; supplementary files) indicating that the sediments did not reach the oil window and were not significantly affected by burial diagenesis (Espitalie et al., 1986). The effect of changes in calcium carbonate and clay mineral composition and contents on the HI values is difficult to establish. The lack of correlation between calcite contents, kaolinite-illite ratios and HI values, opposed to the positive correlation between HI and TOC indicates that stratigraphic changes in HI were due to changes within marine productivity and continental output of OM, rather than by

changes in mineralogy.

Therefore, this method is considered as a valid approximation, which allows interpretation of $\delta^{13}C_{org}$ data that are not related to changes in the source and type of OM, and which might have been driven by regional or even global changes in the carbon cycle instead. Compared to the initial $\delta^{13}C_{org}$ curve, the δ^{13}C-HI index is significantly less noisy and several important shifts were eliminated or diminished by this conversion (Fig. 6).

Within the Hettangian-Sinemurian interval, the bulk-carbonate carbon isotopes were measured on marly samples containing on average 22.5% $CaCO_3$ (Fig. 6). Samples with low carbonate content were eliminated and a minimal threshold value of 10% $CaCO_3$ was respected. The $\delta^{13}C_{carb}$ record correlates well with the δ^{13}C-HI index record both in terms of trends and amplitudes. The two records are therefore assumed to highlight the evolution of the carbon cycle for this region, which is documented in both organic and carbonate reservoirs.

The samples from the interval corresponding to the *jamesoni-ibex* Zones (lower Pliensbachian) have a high average $CaCO_3$ content of around 55%. Through this interval, the $\delta^{13}C_{carb}$ data record a positive shift of +1‰, which is different from the negative shift of around −3‰ observed in the δ^{13}C-HI index and belemnite records (Price et al., 2016). A coeval negative excursion was registered in several other regions in Europe (Korte and Hesselbo, 2011; Duarte et al., 2014; Peti et al., 2016, e.g., Table 1 for a more extensive bibliography) and therefore represent an event of wider extent. Bulk carbonate from this interval of the Dorset section may have been affected by a change in carbonate producers. Alternatively, the pre-shift values may have been diagenetically shifted to more negative values by the incorporation of carbon from originally organic sources. Independently of the mechanism, the corresponding positive carbon-isotope shift cannot be interpreted as a change in the exogenic carbon cycle.

The combination of the δ^{13}C-HI index and the $\delta^{13}C_{carb}$ records shows that the Hettangian-Pliensbachian interval witnessed several perturbations. The most striking shifts are (1) the negative shift which started around the T-J boundary and extended all the way up to the *bucklandi-semicostatum* Zones (lower Sinemurian), (2) the two positive and negative shifts in the Sinemurian; (3) the negative CIE near the Sinemurian-Pliensbachian boundary; and (4) the *margaritatus* positive shift. Two further low-amplitude negative shifts were recorded in the *davoei* Z.-*stokesi* Zones (upper lower to upper Pliensbachian) and *subnodosus* Zone (upper Pliensbachian).

4.3. Marine oxygenation and productivity conditions

In the section of Dorset, marine productivity and oxygenation conditions were determined in order to evaluate the environmental impact of carbon-cycle perturbations, climate change and sea-level variations on the Wessex Basin. Organic-rich sediments are preserved from the Hettangian up to the lower Pliensbachian, and indicate the prevalence of fluctuating oxygen-depleted conditions during this time interval (Hesselbo and Jenkyns, 1995; Hesselbo and Jenkyns, 1998).

The degree of oxygenation was studied using redox-sensitive trace elements (RSTEs), OM content (TOC), hydrogen index (HI) and pyrite content (Fig. 8). The RSTEs used in this study are molybdenum (Mo), uranium (U) and vanadium (V) (Algeo and Maynard, 2004; Tribovillard et al., 2006; Piper and Calvert, 2009; Gertsch et al., 2011).

In the interval between the Hettangian and the lower Pliensbachian (*ibex* Zone) the Mo, U and V records are fluctuating and highly correlated with pyrite content (up to 8%) implying variations in oxygenation conditions (Fig. 8). Mo, U and V contents are enriched in comparison to those in Post-Archaean Average Shale (PAAS) and North American shale composite (NACS) in several layers of this interval. As such, we interpret oxygenation conditions to have varied from dysoxic to anoxic. This is also confirmed by Mo/U and (V/Mo)/Mo plots (Algeo and Tribovillard, 2009; Piper and Calvert, 2009) (Fig. 9). Considering the Mo/U values, some fall within the “particulate shuttle” field (Fig. 9), implying the presence of a Fe−Mn oxyhydroxide shuttle in the water column (Algeo and Tribovillard, 2009). Oxygen-depleted intervals identified here are indicated by blue bands in Fig. 8. The anoxic intervals occurring through the lowermost Jurassic resulted from the strongest oxygen-depleted conditions inferred in this section, as seen from the degrees in RSTE enrichment. The first inferred anoxic interval, occurring right at the T-J boundary (cf. Korte et al., 2009; Page, 2010), was previously detected by measurements of framboidal pyrite and their size (Wignall, 2001). In addition, TOC and HI analysis, were already performed on the same section from the base to the *bucklandi* Zone (Deconinck et al., 2003) and, $\delta^{13}C_{org}$ and TOC analysis were recorded from the *turneri* to the *raricostatum* Zones (Jenkyns and Weedon, 2013). Our results are comparable to and consistent with the results of these important studies.

Interestingly, the uppermost oxygen-depleted event recorded in the lower Pliensbachian (*jamesoni* and *ibex* Zs.) shows enrichment in V, U, TOC and HI, but very low, depleted, Mo values. This is explained by the fact that Mo is less responsive to redox conditions than U and V under suboxic-dysoxic conditions (Lu et al., 2010). This event is therefore interpreted here to have been characterised by suboxic-dysoxic rather than anoxic conditions, unlike the preceding events. This interpretation is supported by the rarity of laminated mudstone within this interval (Jenkyns and Weedon, 2013).

The geochemical record of the succession attributed to the *davoei* and *margaritatus* Zones (Pliensbachian) suggests well-oxygenated conditions (Fig. 8). This interval is characterised by the lowest relative sea level since the Hettangian resulting in quite shallow facies (Hesselbo and Jenkyns, 1998). It is therefore difficult to determine if anoxia ceased in the entire basin or if this setting was not anymore propitious for the development of anoxia because of the shallow environment. Eventually, the evidence for anoxia at this section simply not be preserved, due to missing strata at the hiatus surfaces.

The layers enriched in Mo, U, V and pyrite indicating oxygen-depleted bottom waters coincide with the highest TOC and HI values (maxima of 13 wt% and 710 mg HC/g TOC), which reflect enhanced accumulation and preservation of OM of predominantly marine origin during the time intervals of enhanced oxygen depletion (Fig. 8). The same intervals are also enriched in Cu and Ni, which both are used as productivity proxies (Calvert and Pedersen, 1993; Tribovillard et al., 2004; Tribovillard et al., 2006; Gertsch et al., 2011) (Fig. 8). Consequently, these episodes of oxygen depletion likely relate to phases of enhanced marine primary productivity.

As limestones were often avoided, a sample-related bias may be considered. The carbonates alternating with the shally intervals reflects periods with improved oxygenated conditions (e.g., Weedon and Jenkyns, 1999).

4.4. Climate conditions

Changes within the CIA index reflect the importance of plagioclase leaching on the continent and are generally interpreted in terms of weathering intensity and therefore of humidity conditions on the adjacent land (Nesbitt and Young, 1982, 1989). The results obtained at Dorset indicate that the Hettangian and the Sinemurian are characterised by a more humid climate than the Pliensbachian (Fig. 7). This general trend was not uniform but was modulated by shorter intervals with slightly drier or more humid conditions.

Clay minerals in the Dorset section were not too strongly affected by diagenetic replacement or neoformation and are therefore useful for palaeoclimatic recontructions, as was already shown by Deconinck et al. (2003). This is confirmed by the low Tmax values (around 422 °C) showing the absence of a strong burial diagenetic overprint (Fig. S1 - supplementary files) (Espitalie et al., 1986).

The clays contain smectite, illite, chlorite, kaolinite and illlite/smectite mixed layers (Figs. 5, 8), which were derived from the nearby Hercynian massifs surrounding the Wessex and the Bristol Channel

Table 1
Compilation of the localities, carbon carrier, amplitudes and references from the studies recording carbon isotopic events during the Hettangian -Pliensbachian time interval.

$\delta^{13}C$ events	C carrier	Locality	$\delta^{13}C$ CIE amplitude	References
N Main CIE (Late Raethian-Hettangian-Earliest Sinemurian)	Bulk OM	USA	2–2.5‰	Guex et al., 2004; Ward et al., 2006; Bartolini et al., 2012
		Peru	2‰	Yager et al., 2017
		Italy	3.5‰	Bachan et al., 2012
		Germany	3–5‰	Quan et al., 2008a, 2008b; Van de Schootbrugge et al., 2013
		Austria	3–5‰	Kuerschner et al., 2007; Bonis et al., 2009; Ruhl et al., 2009
		UK	3–5‰	Hesselbo et al., 2002, Ruhl et al., 2010; Clémence et al., 2010; This study
	OM HI-corrected	UK	5‰	This study
	Wood	Denmark (Greenland)	3‰	McElwain et al., 1999
	Bulk carbonate	Montenegro	1‰	Črne et al., 2011
	Other calcitic organisms	UK	2.5–3‰	Korte et al., 2009
Turneri N CIE (Early Sinemurian)	Bulk OM	UK	2‰	Jenkyns and Weedon, 2013; This study
	OM HI corrected	UK	< 1‰	This study
	Bulk carbonate	UK	2‰	This study
Obusum N CIE (Late Sinemurian)	Bulk OM	UK	3.5‰	Jenkyns and Weedon, 2013; This study
	OM HI corrected	UK	2‰	This study
	Bulk carbonate	UK	2.5‰	Van de Schootbrugge et al., 2005; This study
Oxynotum N CIE (Late Sinemurian)	Bulk OM	France	2.5‰	Peti et al., 2016
		UK	2–3‰	Riding et al., 2012
	Palynomorphs	UK	2–3‰	Riding et al., 2012
	Bulk carbonate	UK	3‰	Van de Schootbrugge et al., 2005
	Belemnites	UK	2–3‰	Riding et al., 2012
Raricostatum P CIE (Late Sinemurian)	Bulk OM	UK	2–4‰	Riding et al., 2012; Jenkyns and Weedon, 2013; This study
	OM HI corrected	UK	2‰	This study
	Wood	UK	2–3‰	Korte and Hesselbo, 2011
	Palynomorphs	UK	2–3‰	Riding et al., 2012
	Bulk carbonate	UK	2‰	This study
	Belemnites	UK	2–3‰	Korte and Hesselbo, 2011; Riding et al., 2012
	Other calcitic organisms	UK	2–3‰	Korte and Hesselbo, 2011
Sinemurian-Pliensbachian boundary N CIE	Bulk OM	UK	3–4‰	Van de Schootbrugge et al., 2005, this study
		France	2–4‰	Peti et al., 2016; Mercuzot et al., 2019
		Morocco	3‰	Mercuzot et al., 2019
		Canada		Caruthers et al., 2014
	OM HI-corrected	UK	2‰	this study
	Wood	UK	4‰	Korte and Hesselbo, 2011
		Portugal		Suan et al., 2010
	Bulk carbonate	UK	2‰	Van de Schootbrugge et al., 2005
		Morocco	2‰	Mercuzot et al., 2019
		France	1–1.5‰	Bougeault et al., 2017; Mercuzot et al., 2019
		Portugal	2–3‰	Oliveira et al., 2006; Duarte et al., 2014
		Italy	1.5–3‰	Morettini et al., 2002; Speranza and Parisi, 2007; Woodfine et al., 2008; Marino and Santantonio, 2010; Franceschi et al., 2014
		Switzerland		Schöllhorn et al., in prep. - chapter 3
	Belemnites	UK	3‰	Korte and Hesselbo, 2011; Price et al., 2016
		Spain	1–3‰	Rosales et al., 2006; Armendáriz et al., 2012; Gómez et al., 2016
	Other calcitic organisms	UK	4‰	Korte and Hesselbo, 2011
		Portugal	2.5‰	Suan et al., 2010
Upper Pliensbachian P CIE	Bulk OM	UK	3.5–6‰	Van de Schootbrugge et al., 2005;This study
		Morocco	4‰	Mercuzot et al., 2019
		France	5‰	Peti et al., 2016; Mercuzot et al., 2019
		Canada and USA	3‰	Caruthers et al., 2014
	OM HI corrected	UK	3.5‰	This study
	Wood	UK	8‰	Korte and Hesselbo, 2011
		Portugal	3‰	Suan et al., 2010
	Bulk carbonate	UK	2.5–4‰	Van de Schootbrugge et al., 2005
		Portugal	2‰	Oliveira et al., 2006; Silva et al., 2011
		Morocco	3‰	Mercuzot et al., 2019
		France	2‰	Van de Schootbrugge et al., 2010; Harazim et al., 2013
		Italy	1.5‰	Morettini et al., 2002; Speranza and Parisi, 2007; Woodfine et al., 2008; Marino and Santantonio, 2010
		Switzerland	> 1.5‰	Jenkyns and Clayton, 1986; Schöllhorn et al., 2019.
	Belemnites	UK	4‰	Bailey et al., 2003; Korte and Hesselbo, 2011; Price et al., 2016
		Spain	2.5–3.5‰	Rosales et al., 2004; Gómez et al., 2016
	Other calcitic organisms	UK	4‰	Korte and Hesselbo, 2011
		Portugal	3‰	Suan et al., 2010

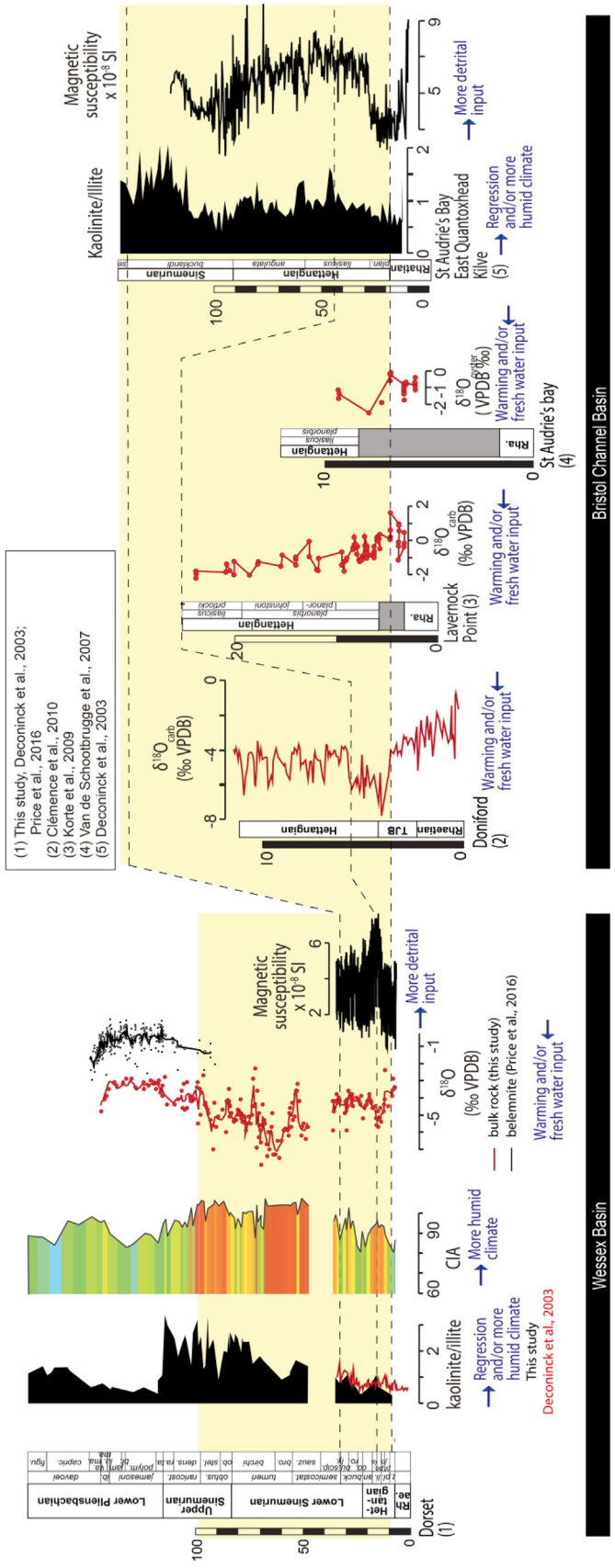

Fig. 10. Review of climate proxies from the Hettangian to the early Sinemurian across the Wessex and the Bristol Channel Basins (England) ($\delta^{18}O_{carb}$: oxygen isotopes performed on bulk carbonate; CIA: alteration index based on the methodology described by Nesbitt and Young, 1982, 1989). P means positive and N negative.

Basins. However, as the clay assemblage contains really low smectite content they unlikely came from the smectite-rich Welsh and London-Brabant Massifs but rather from the Armorican and Cornubian Massifs (Ziegler, 1990; Bradshaw et al., 1992; Deconinck et al., 2003).

In marine environments the clay composition is modulated by climate and sea level variations. The latter may fractionate clay minerals because of different settling characteristics. For example, kaolinite is less well transported to distal areas than other clay minerals because of its relatively rapid settling, and kaolinite-rich assemblages may represent more proximal environments and vice versa (Parkinson, 1996; Godet et al., 2008). Kaolinite-rich assemblages may also represent periods of more intense chemical weathering on the continent because of a change to a warmer and more humid climate (Chamley, 1989; Velde, 1995; Thiry, 2000; Deconinck et al., 2003). In the Dorset exposures the clay-mineral composition appears to have been controlled alternatively by one of these mechanisms or by both. For instance, the higher kaolinite:illite (K:I) ratios recorded during the Hettangian and Sinemurian in comparison to the upper Pliensbachian have not been driven by sea-level change, since these sediments were deposited in more distal environments (sensu Hesselbo and Jenkyns, 1998). High K/I is therefore considered to reflect warmer and more humid conditions, which is also indicated by the CIA (Fig. 7). In addition, the two low-amplitude K/I increases recorded in the middle Hettangian and the *bucklandi* Zone (lower Sinemurian) probably reflect changes to even more humid climate conditions as is also shown by the good correlation with increased CIA values (Fig. 7) and by the study of Deconinck et al. (2003). In contrast, the long-term increase in the K/I ratio from the Hettangian through to the upper Sinemurian and the abrupt decrease near the Sinemurian-Pliensbachian boundary are controlled at least in part by sea-level rise and fall, which occurred during this time (Fig. 7). This is suggested by the good correlation with the sea-level variations reconstructed by Hesselbo and Jenkyns (1998).

In the Wessex basin, the assemblages may have also been influenced by marine transgression and subsequent reworking of illitic material from Hercynian rocks during fault activity (Deconinck et al., 2003). Several studies indicate Early Jurassic fault movements in the Wessex basin (Chadwick, 1986; Jenkyns and Senior, 1991) but their chronology is poorly known and precise correlations are not possible. However, the clay composition correlates generally rather well with the CIA and sea-level trends, thus indicating an environmental rather than a tectonic control.

In addition, kaolinite precipitated authigenically during early diagenesis and controlled the clay mineralogical composition during part of the Sinemurian interval in the neighbouring Cleveland Basin (Hesselbo et al., 2019). This mechanism occurred in coarser grained sediments where the original muscovite content was highest. However, in the Dorset record the highest kaolinite content is recorded in the Hettangian-Sinemurian sediments which are characterised by finer grainsize and lower detrital content compared to the upper Pliensbachian which records the coarsest grains, the highest detrital content and lower kaolinite content. Therefore, the overall decreasing kaolinite:illite trend cannot be explained by this mechanism. In some short-term intervals it may have had some influence.

The oxygen-isotope record was considered from the base of the section up to the interval corresponding to the *ibex* Zone (lower Pliensbachian) (Fig. 7). This time interval witnessed several $\delta^{18}O$ shifts, which may be explained by one or a combination of the following mechanisms (Emiliani, 1955; Shackleton, 1967; Raymo et al., 1989; Zachos et al., 2001; Föllmi, 2012):

(1) temperature change of the water column;
(2) variations in fresh-water input linked to changes in the hydrological cycle and humidity on the adjacent continent;
(3) changes in the source of carbonate;
(4) changes in diagenetic overprint.

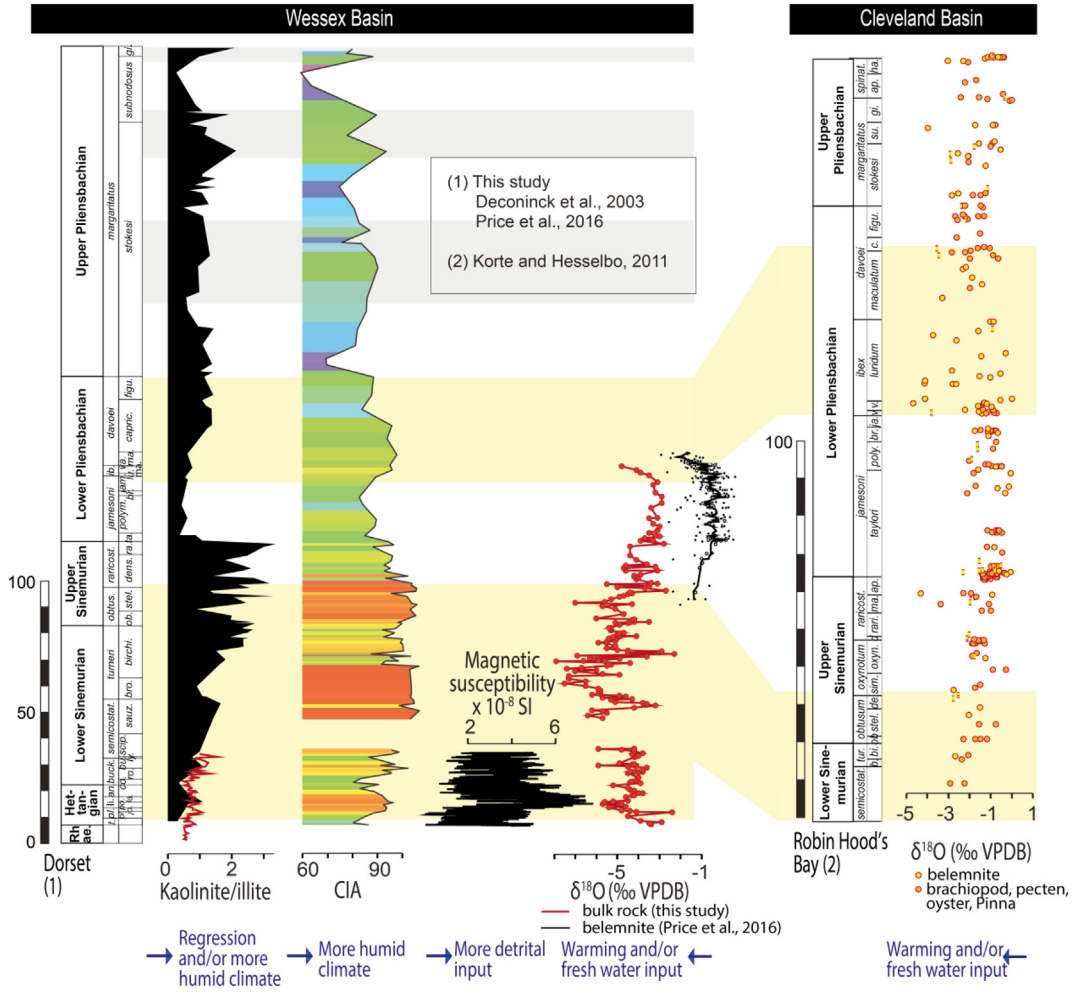

Fig. 11. Review of climate proxies from the Hettangian to the Pliensbachian across the Wessex and Cleveland Basins ($\delta^{18}O_{carb}$ and $\delta^{18}O_{belm}$: oxygen isotopes performed on bulk carbonate and belemnites (Price et al., 2016); CIA: alteration index based on the methodology described by Nesbitt and Young, 1982, 1989; Mg: Magnesium; Ca: Calcium; Sr: Strontium).

Global temperatures during the Early Jurassic were considered to be generally warm, 5–10 °C higher than today, and the presence of substantial ice sheets was rather limited (Chandler et al., 1992; Sellwood and Valdes, 2008; Dera et al., 2009a, 2009b, 2011; Ruebsam et al., 2019). Ruebsam et al. (2019) proposed an ice-house interval during the late Pliensbachian. However, the time interval spanning the $\delta^{18}O$ record (Hettangian - lower Pliensbachian) is rather characterised by a greenhouse climate as no unequivocal evidence for ice sheets was described. A glacio-eustatic control on the oxygen-isotope record is therefore less likely.

The oxygen-isotope data range between −7 and − 2‰, which is more negative than usual (e.g., Van de Schootbrugge et al., 2005; Oliveira et al., 2006). It is therefore possible that diagenetic overprint has shifted the data set to more negative values. However, when comparing our results with the data from belemnites for the Sinemurian-Pliensbachian boundary interval in the same section (Price et al., 2016), and with other British records obtained on oysters and bulk carbonate for the early Hettangian (Doniford, Clémence et al., 2010; Lavernock Point, Korte et al., 2009; St. Audrie's Bay, Van de Schootbrugge et al., 2007) the trends are highly coherent (Figs. 10 and 11). We therefore consider the oxygen-isotope record to preserve an environmental signal for at least the lower Hettangian and the upper Sinemurian-lower Pliensbachian intervals (Fig. 7). In the intervals in between, diagenetic overprint may have been more important. The negative oxygen-isotope shifts correlate significantly with the more humid intervals determined by a higher CIA index and K:I ratios and are explained here to reflect at least in part by increased fresh water input (Fig. 7).

During the Hettangian-earliest Sinemurian, intervals with higher CIA values and K:I ratios coincide with higher magnetic susceptibility measured in the same Dorset section, and in the adjoining Bristol Channel Basin (Deconinck et al., 2003) may be interpreted as an indicator of higher detrital input. This would fit well with our interpretation of more humid conditions during this time interval (Fig. 10). Furthermore, oxygen isotope data obtained on belemnites and other calcitic organisms from the Cleveland Basin, show correlatable trends with lower values in the lower Sinemurian and in the *ibex* and *davoei* Zones, and higher values in the lowermost Pliensbachian (Fig. 11; Hesselbo et al., 2000; Korte and Hesselbo, 2011).

Together with the available published data, our new palaeoclimate record highlights the importance of warm and more humid conditions during the Hettangian-Sinemurian (up to the *obtusum* Zone) interval and less humid conditions during the Pliensbachian interval (Figs. 7, 10, 11). The period of increased humidity during the Hettangian-Sinemurian was not uniform but modulated by intervals with slightly drier conditions. The early Pliensbachian recorded drier and cooler conditions during the *jamesoni-ibex* Zones and more humid conditions during the *davoei* Zone. The *margaritatus* Zone is characterised by drier conditions with some intervals of higher humidity. More humid conditions were inferred at the base of the *jamesoni* Zone in the Cleveland Basin (Van Buchem et al., 1992) and in the Cardigan Bay Basin (Deconinck et al., 2019) – in an interval, which may be missing at

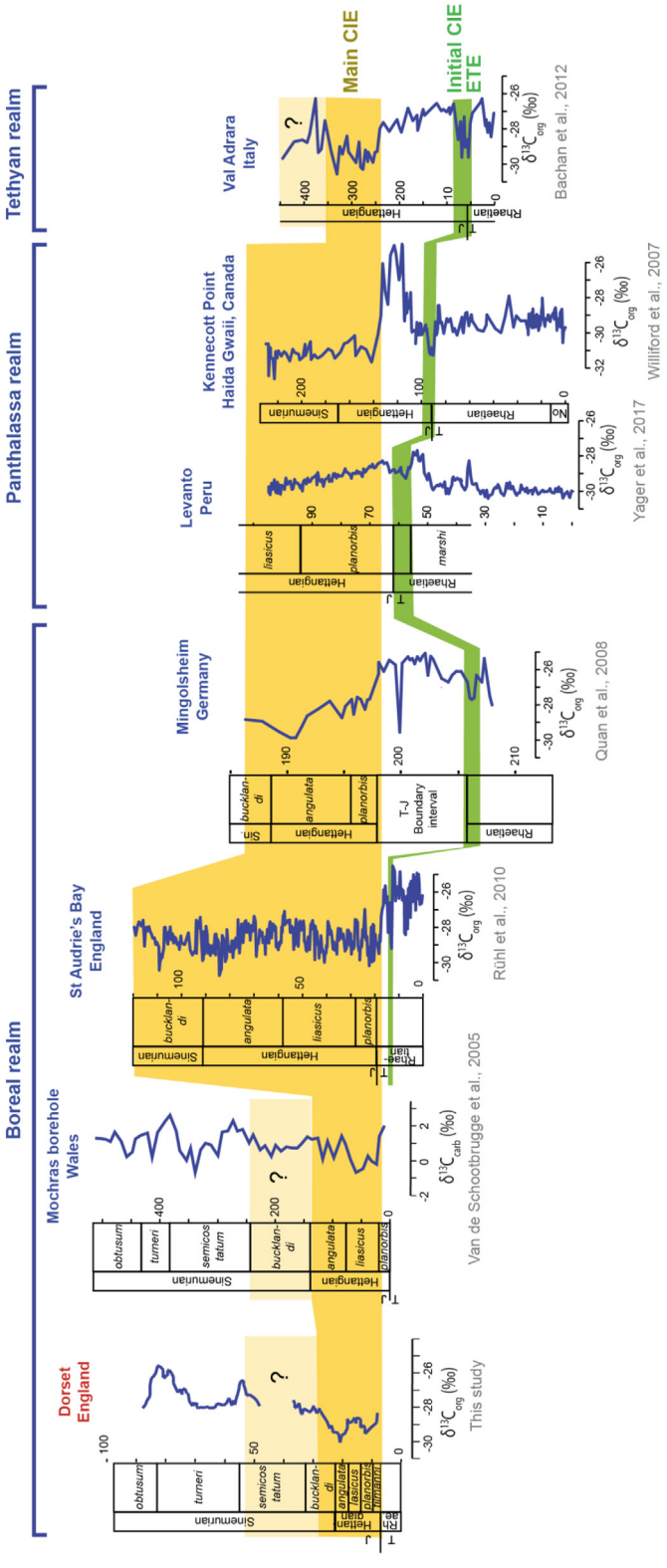

Fig. 12. Compilation and correlation of carbon-isotope data recording the main CIE.

Dorset because of a hiatus (Hesselbo and Jenkyns, 1998). The study performed on the Cardigan Bay Basin did also record an increase in the K:I ratio in the *davoei* Zone, which is consistent with the Dorset record.

4.5. Correlations and global implications

4.5.1. The carbon-isotope records

A comparison of the Dorset $\delta^{13}C_{org}$ record with a compilation of published carbon-isotope data from the British realm and other basins within and outside Europe (see compilation in Table 1; Figs. 12 and 13) suggests that the main trends in the carbon-isotope record are of wider significance. Larger, consistently recorded shifts correspond to (1) the negative main CIE (earliest Jurassic); (2) the negative Sinemurian-Pliensbachian boundary CIE; and (3) the positive CIE of the *margaritatus* Zone. Other excursions are common in the British realm but it is not yet possible to evaluate their true importance because of insufficient records (e.g., negative CIEs of the *turneri*, *obtusum*, and *davoei-lower margaritatus* Zones).

This compilation of carbon-isotope records provides compelling evidence that during the Hettangian-Pliensbachian interval the carbon cycle, and the general climate conditions, were not stable but rather fluctuating. A clear reference value, which would allow identification and definition of background conditions, appears to be lacking, and the records seem instead to be characterised by a continuously changing carbon cycle. These fluctuations render it difficult to determine which trends are related to events and which ones are related to a return to initial values due to cessation of the causal mechanism.

Some debate on the globality and existence of the main CIE has arisen (cf. Hesselbo et al., 2002). It is unclear if the main CIE corresponds to (a) a return to background values after a positive shift recorded around the T-J boundary (Williford et al., 2007; Van de Schootbrugge et al., 2007) or (b) to a true negative excursion related to a late phase of Central Atlantic Magmatic Province (CAMP) activity (Ruhl et al., 2016) (Fig. S4; supplementary files). Indeed, most of the $\delta^{13}C$ records were performed on bulk organic matter (Table 1), which changed from mainly continental (uppermost Triassic) to mainly marine organic matter (Lower Jurassic), eventually due to a global transgressive trend (Hallam, 1988; Haq, 2017). As changes in the organic matter type may induce shifts in the $\delta^{13}C_{org}$ record (Suan et al., 2015), it is difficult to evaluate if the $\delta^{13}C$ values of the exogenic reservoirs during the main CIE are truly more negative than the average $\delta^{13}C$ values of the upper Rhaetian. Two records were generated from bulk carbonate and calcitic organisms (UK - Korte et al., 2009; Montenegro - Črne et al., 2011) which show more negative $\delta^{13}C$ values during the main CIE in comparison to the upper Rhaetian sediments. However, further analyses are needed to confirm this. In addition, the efficiency of the carbon pump may have also influenced the length of this event. With an inefficient carbon pump, related to a carbonate crisis, even a short-term input of light carbon may have led to a longer return to normal values.

Independently, the $\delta^{13}C$ records from the section of St. Audrie's Bay (England) and the Mingolsheim core (Germany) suggest that the main CIE extended well into the lower Sinemurian (*bucklandi* Zone) without reaching its end (Fig. 12; Quan et al., 2008a, 2008b; Ruhl et al., 2010). The Mochras core, Cardigan Bay Basin, (Van de Schootbrugge et al., 2005) and our study show the most negative $\delta^{13}C$ values through the Hettangian and the termination of the main CIE is not clearly identifiable, but is located somewhere between the Hettangian-Sinemurian boundary and the *semicostatum* Zone (lower Sinemurian). As the Hettangian may have had a duration of 2 Myr (Ruhl et al., 2010) or even 4.1 Myr (Weedon et al., 2018) and the *bucklandi* Zone of > 1.1 Myr, the more negative $\delta^{13}C$ values were recorded during the main CIE during several million years (> 3 Myr) in the British and German realms.

The duration of the Sinemurian-Pliensbachian CIE was estimated as 2 million years at Robin Hood's Bay (Ruhl et al., 2016). In the Dorset section and in Spain (Fig. 13; Quesada et al., 2005; Gómez et al., 2016) it appears that this event lasted beyond the *jamesoni* Zone, until the *ibex* Zone. This, if confirmed in other basins, implies that the duration of this event is longer than 2.7 (± 0.15) Myr, which is the length of the *jamesoni* Zone estimated by Ruhl et al., 2016.

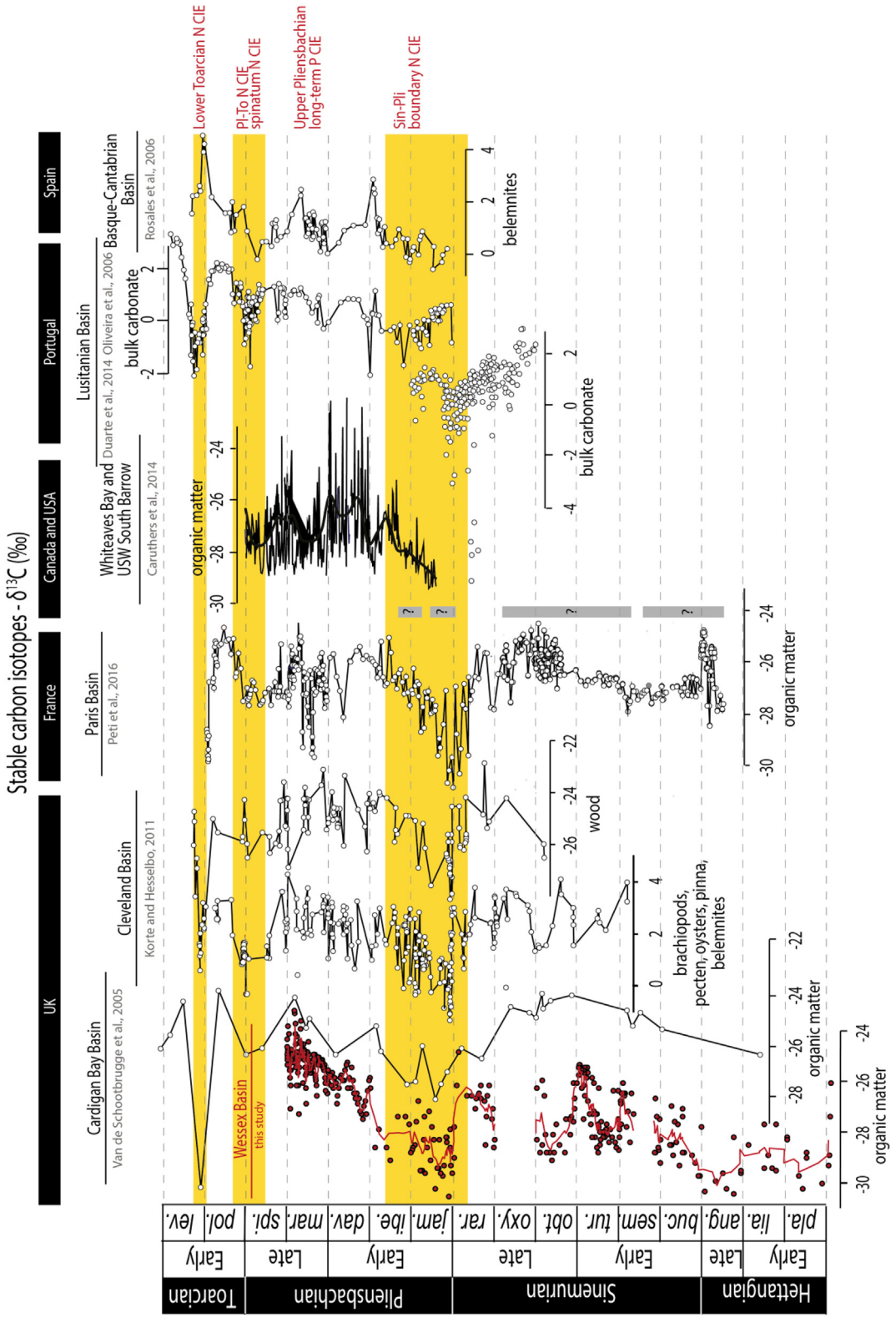

Fig. 13. Compilation and correlation of carbon-isotope records from the Lower Jurassic across different basins.

The Sinemurian-Pliensbachian event was related to a late phase of CAMP volcanic activity (e.g., Ruhl et al., 2016), and/or to the opening of the Hispanic corridor (Franceschi et al., 2014; Porter et al., 2013) (Fig. S4; supplementary files). Alternatively, Danisch et al. (2019) explained this CIE by the return to background values following a positive late Sinemurian CIE. Given the very low $\delta^{13}C$ values reached during the Sinemurian-Pliensbachian CIE, which represent the lightest values measured not only in the entire section in Dorset, but also in most other sections (Fig. 13), we prefer an interpretation of reinforced input of light carbon into the exogenic reservoirs as a driver of this important negative CIE. However, the $^{40}Ar/^{39}Ar$ data that provides evidence for Early Jurassic volcanism were mostly generated several years ago using

methodologies including large uncertainty with regards to the age determination. Therefore, the correlation with late phases of CAMP volcanism remains speculative.

The general positive $\delta^{13}C$ shift of the late Pliensbachian (*davoei* to *margaritatus* Zones) has been related to increased OM preservation in the Lusitanian, Basque Cantabrian and Asturian Basins (Aurell et al., 2003; Quesada et al., 2005; Duarte et al., 2010; Silva et al., 2010, 2011; Armendáriz et al., 2012; Caruthers et al., 2014). Contemporaneous organic-rich intervals are also known from western Canada (Riediger, 2002; Asgar-Deen et al., 2003; Them II et al., 2017, Them II et al., 2018), France (Bessereau et al., 1995; Léonide et al., 2007; Van de Schootbrugge et al., 2010), Austria (Kodina et al., 1988) and from Siberia, northeastern Russia, the Canadian Arctic and the Arctic platform of Alaska (Nikitenko and Mickey, 2004). The positive *margaritatus* Z. CIE may indeed be related to a period of enhanced OM burial and preservation. In the same time, volcanic activity as a source of light carbon may have diminished and exogenic changes in the carbon cycle may thus have had a large influence on changing the $\delta^{13}C$ record. Previous periods of likely increased organic-carbon burial during the Hettangian to early Pliensbachian were rather linked to negative CIEs, at least in Dorset (Fig. 8).

4.5.2. Climate, humidity and anoxia

Fluctuating anoxic conditions were not only recorded at Dorset but also at Doniford in the adjacent Bristol Channel Basin for the Hettangian, based on TOC contents (5–10%) and the absence of benthic foraminifers (Clémence et al., 2010). Based on TOC contents (up to 13%), high HI values and palynological evidence (*Tasmanites*, amorphous OM, acritarch abundances; Fig. 14), similar conditions were also described from other locations in the Bristol Channel Basin (Hettangian-earliest Sinemurian; Hesselbo et al., 2002; Van de Schootbrugge et al., 2007; Ruhl et al., 2010; Jaraula et al., 2013; Hüsing et al., 2014; Xu et al., 2016). In contrast, sections from the neighbouring Cleveland and Cardigan Bay Basins document environments in which the degree of deoxygenation was dysoxic at most (based on TOC and V contents and HI values; Van Buchem et al., 1992; Van de Schootbrugge et al., 2005). It is therefore likely that the Wessex and Bristol Channel Basins were more restricted and more sensitive to develop anoxic conditions as the consequence of propitious climate and sea-level conditions.

The establishment of strongly fluctuating anoxic conditions in the Wessex and Bristol Channel Basins from the Hettangian to the Sinemurian points to a combination of favourable parameters related to restricted circulation, high sea-level and increased runoff during wetter climates (e.g., CIA, $\delta^{18}O$ and clays) leading to increased nutrient and fresh-water input, as was already stated by Jenkyns and Weedon (2013). These factors prompted higher productivity and preservation of marine OM leading to the formation of the darker, laminated and more clay-rich sediments. The more humid climate was modulated by Milankovich cycles for the Hettangian – lowermost Sinemurian (*bucklandi* Zone) at least (Blue Lias; Weedon, 1986; Fleet et al., 1987; Hesselbo et al., 2002; Van de Schootbrugge et al., 2007; Clémence et al., 2010; Ruhl et al., 2010; Hüsing et al., 2014; Xu et al., 2016; Weedon et al., 2017).

Oxygen depleted conditions were also recorded from several basins outside the British realm, but they were mostly restricted to the earliest Hettangian. Strongly reducing conditions were documented in Luxembourg (Richoz et al., 2012), the North German Basin (Heunisch et al., 2010; Richoz et al., 2012; Luo et al., 2018), the South German Basin (Quan et al., 2008a, 2008b; Van de Schootbrugge et al., 2013; Luo et al., 2018), the Swiss Jura mountains (Schwab et al., 2006) and in west Canada (Kasprak et al., 2015). Organic-rich shales that may suggest oxygen-depleted conditions were recorded on marine and continental basins in the Apennine Basin (Ciarapica, 2007), Pucara Basin (Szekely and Grose, 1972), Newark Basin (Olsen et al., 1996; Olsen and Kent, 1999), Hartford Basin (Olsen et al., 1989), Deerfield Basin (Olsen et al., 1989) and New York Canyon Basin (Guex et al., 2004).

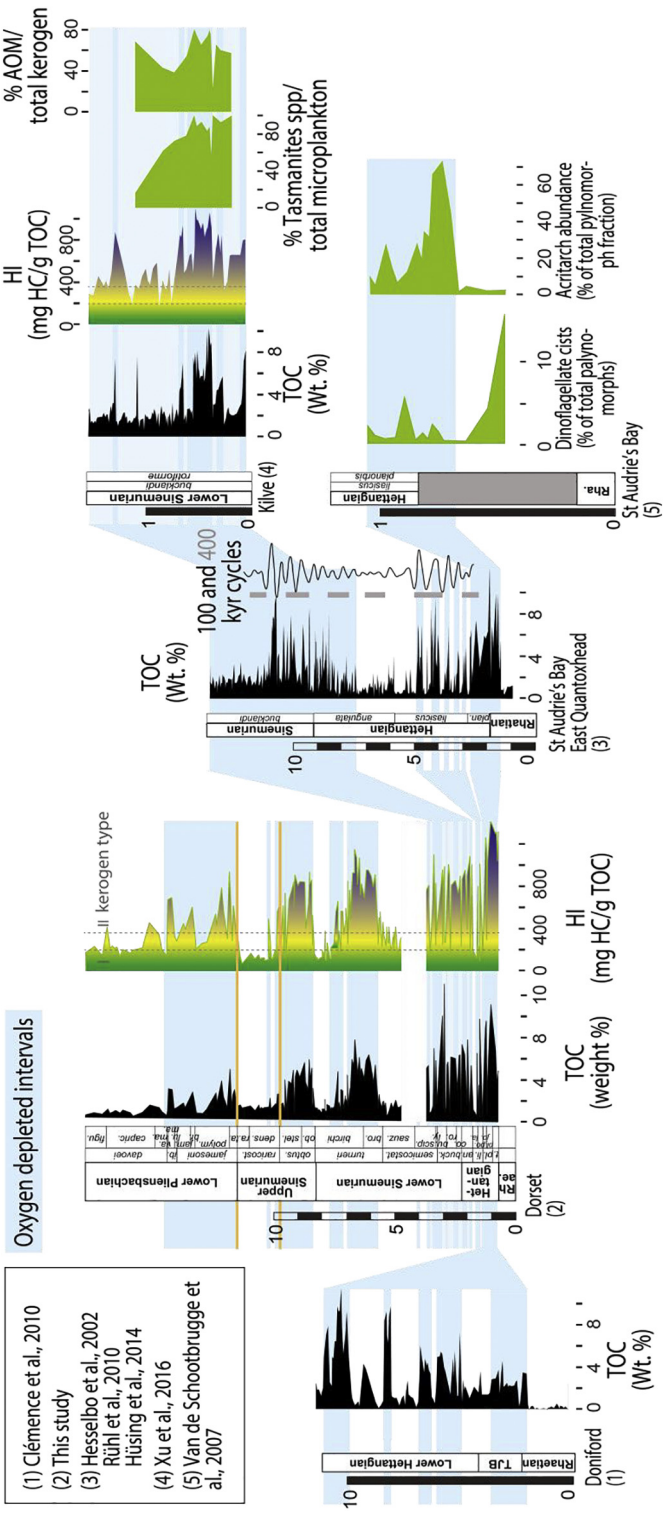

Fig. 14. Compilation of marine oxygenation proxies across different basins from the British realm (TOC: total organic carbon; HI: hydrogen index).

In contrast to the Hettangian-Sinemurian oxygen-depleted episodes, the one recorded during the earliest Pliensbachian (*jamesoni* and *ibex* Zones) correlates with drier (e.g. CIA and clay mineralogy) and eventually also cooler conditions (e.g., oxygen isotopes; Price et al., 2016). Even if this episode is characterised by less deoxygenated conditions in the water column than the previous occurrences, it still suggests that conditions remain favourable for the set-up of oxygen depletion in spite of the less propitious climate circumstances.

The increased humidity during the Hettangian-Sinemurian relative to the Pliensbachian is explained here by one or a combination of two mechanisms:

(1) High atmospheric pCO_2 related to increased emissions of greenhouse gases resulting from increased rifting and late CAMP volcanism (Fig. S4; supplementary files) may have controlled the Hettangian-Sinemurian climate. Late CAMP volcanism during the Early Jurassic is evidenced by $^{39}Ar/^{40}Ar$ ages of related deposits and intrusions (summarized in Ruhl et al., 2016), strontium isotopes (Jones et al., 1994; Ruhl et al., 2016), osmium isotopes (Cohen et al., 1999; Cohen and Coe, 2002; Cohen et al., 2004; Kuroda et al., 2010), leaf physiognomy and palynological studies (Mander et al., 2013; Bacon et al., 2013). However, increased tectonic and volcanic activity related to an ultimate phase of CAMP or early phases of the Karoo-Ferrar LIP may have persisted through the Pliensbachian (Caruthers et al., 2014; Ruhl et al., 2016).
(2) The long-term trend in palaeoclimatic change coincides more specifically with the opening of the Hispanic corridor around the Sinemurian-Pliensbachian boundary (Damborenea and Manceñido, 1979; Hallam, 1983; Smith, 1983; Smith and Tipper, 1986; Smith et al., 1990; Aberhan, 2001; Arias, 2006, 2007; Venturi et al., 2006, 2007; Porter et al., 2013; Franceschi et al., 2014). The Viking strait also opened during the Early Jurassic but its timing is less well known. The first fully marine strata established in the Jameson Land Basin of East Greenland may provide evidence for increasing northward marine connectivity at the Sinemurian-Pliensbachian stage boundary (Surlyk, 2003; Korte and Hesselbo, 2011). However, other studies dated the opening of the Viking strait at the end of the Pliensbachian (Bjerrum et al., 2001; Van de Schootbrugge et al., 2005). In addition, the *davoei* Zone (Lower Pliensbachian) interval coincides with a positive εNd excursion (Dera et al., 2009a, 2015) evidencing an incursion of warm-water masses from the equatorial Tethys (Fig. S4; supplementary files). These significant changes in palaeogeographic and current pattern may have also impacted regional climate conditions. Therefore, the changes recorded at Dorset do probably not only reflect carbon cycle perturbations but also this geographically deeply changing world. Within the Pliensbachian short-lived climate snaps were not only recorded in the British realm but were also reported by Silva and Duarte (2015) and Peti and Thibault (2017).

5. Conclusions

New geochemical and mineralogical data are provided from the Hettangian to Pliensbachian section of Lyme Regis and Charmouth along the Dorset coast (UK) allowing to a substantial improvement in knowledge of the marine oxygenation and productivity conditions and the associated climatic changes in the Wessex Basin. As already shown for the Sinemurian interval itself (Jenkyns and Weedon, 2013) several episodes of strongly oxygen-depleted conditions (HI, Mo, U, V, TOC and pyrite content) were recorded during the Hettangian – Sinemurian interval which were each linked to high productivity (Cu, Ni, TOC and HI) and increased fresh-water input to the seaway. These episodes were related to increased runoff caused by a warm and more humid climate (CIA, clay mineralogy, $\delta^{18}O$).

The Pliensbachian is generally characterised by a drier climate but with shorter intervals of higher humidity during the *davoei* and *margaritatus* Zones. The long-term trend towards less humid conditions through the Hettangian-Pliensbachian is interpreted to have resulted from (1) variations in the position of climate belts related to changes in palaeogeography and current pattern due to the break-up of Pangaea and, with that, the Hispanic Corridor around the Sinemurian-Pliensbachian boundary; and/or (2) changes in the intensity of volcanic and rifting activity leading to variations in the atmospheric CO_2 content.

Acknowledgements

We would like to acknowledge the logistical and financial support of the University of Lausanne. We thank both Tiffany Monnier and Jean-Claude Lavanchy for their assistance in the laboratories, Nikki Szerkowski for the help on the field as well as Jorge Spangenberg for his help and important input with regard to the analysis of carbon and oxygen isotopes. Furthermore, we would like to acknowledge Steve Hesselbo and one anonymous reviewer for their constructive advice that improved this study considerably.

Appendix A. Supplementary data

Supplementary data to this article can be found online at https://doi.org/10.1016/j.gloplacha.2019.103096.

References

Aberhan, M., 2001. Bivalve palaeobiogeography and the Hispanic Corridor: time of opening and effectiveness of a proto-Atlantic seaway. Palaeogeogr. Palaeoclimatol. Palaeoecol. 165 (3–4), 375–394.
Adatte, T., Stinnesbeck, W., Keller, G., 1996. Lithostratigraphic and mineralogic correlations of near K/T boundary clastic sediments in northeastern Mexico: implications for origin and nature of deposition. Geol. Soc. Am. Spec. Pap. 307, 211–226.
Algeo, T.J., Maynard, J.B., 2004. Trace-element behavior and redox facies in core shales of Upper Pennsylvanian Kansas-type cyclothems. Chem. Geol. 206 (3–4), 289–318.
Algeo, T.J., Tribovillard, N., 2009. Environmental analysis of paleoceanographic systems based on molybdenum-uranium covariation. Chem. Geol. 268 (3–4), 211–225.
Anders, E., Grevesse, N., 1989. Abundances of the elements: meteoritic and solar. Geochim. Cosmochim. Acta 53 (1), 197–214.
Arabas, A., Schlögl, J., Meister, C., 2017. Early Jurassic carbon and oxygen isotope records and seawater temperature variations: insights from marine carbonate and belemnite rostra (Pieniny Klippen Belt, Carpathians). Palaeogeogr. Palaeoclimatol. Palaeoecol. 485, 119–135.
Arias, C., 2006. Northern and Southern Hemispheres ostracod palaeobiogeography during the early Jurassic: possible migration routes. Palaeogeogr. Palaeoclimatol. Palaeoecol. 233 (1–2), 63–95.
Arias, C., 2007. Pliensbachian–Toarcian ostracod biogeography in NW Europe: evidence for water mass structure evolution. Palaeogeogr. Palaeoclimatol. Palaeoecol. 251 (3–4), 398–421.
Armendáriz, M., Rosales, I., Bádenas, B., Aurell, M., García-Ramos, J.C., Piñuela, L., 2012. High-resolution chemostratigraphic records from lower Pliensbachian belemnites: Palaeoclimatic perturbations, organic facies and water mass exchange (Asturian basin, northern Spain). Palaeogeogr. Palaeoclimatol. Palaeoecol. 333-334, 178–191.
Asgar-Deen, M., Hall, R., Craig, J., Riediger, C., 2003. New biostratigraphic data from the lower Jurassic Fernie Formation in the subsurface of west-Central Alberta and their stratigraphic implications. Can. J. Earth Sci. 40 (1), 45–63.
Aurell, M., Robles, S., Bádenas, B., Rosales, I., Quesada, S., Meléndez, G., Garcıa-Ramos, J., 2003. Transgressive–regressive cycles and Jurassic palaeogeography of Northeast Iberia. Sediment. Geol. 162 (3–4), 239–271.
Bachan, A., Schootbrugge, B., Fiebig, J., McRoberts, C.A., Ciarapica, G., Payne, J.L., 2012. Carbon cycle dynamics following the end-Triassic mass extinction: constraints from paired δ13Ccarb and δ13Corg records. Geochem. Geophys. Geosyst. 13 (9).
Bacon, K.L., Belcher, C.M., Haworth, M., McElwain, J.C., 2013. Increased atmospheric SO2 detected from changes in leaf physiognomy across the Triassic–Jurassic boundary interval of East Greenland. PLoS ONE 8 (4), e60614.
Bailey, T.R., Rosenthal, Y., McArthur, J.M., Van de Schootbrugge, B., Thirlwall, M.F., 2003. Paleoceanographic changes of the late Pliensbachian–early Toarcian interval: a possible link to the genesis of an Oceanic Anoxic Event. Earth Planet. Sci. Lett. 212 (3–4), 307–320.
Bartolini, A., Guex, J., Spangenberg, J.E., Schoene, B., Taylor, D.G., Schaltegger, U., Atudorei, V., 2012. Disentangling the Hettangian carbon isotope record: Implications for the aftermath of the end-Triassic mass extinction. Geochem. Geophys. Geosyst. 13 (1).
Behar, F., Beaumont, V., Penteado, H.D.B., 2001. Rock-Eval 6 technology: performances and developments. Oil Gas Sci. Technol. 56 (2), 111–134.
Bessereau, G., Guillocheau, F., Huc, A.-Y., 1995. Source rock occurrence in a sequence stratigraphic framework: the example of the Lias of the Paris Basin. Am. Assoc. Petrol. Geol. Spec. Vol. 40, 273–301.
Bjerrum, C.J., Surlyk, F., Callomon, J.H., Slingerland, R.L., 2001. Numerical paleoceanographic study of the early Jurassic transcontinental Laurasian Seaway. Paleoceanography 16 (4), 390–404.
Blackburn, T.J., Olsen, P.E., Bowring, S.A., McLean, N.M., Kent, D.V., Puffer, J., McHone, G., Rasbury, E.T., Et-Touhami, M., 2013. Zircon U-Pb geochronology links the end-Triassic extinction with the Central Atlantic Magmatic Province. Science 340 (6135), 941–945.
Blakey, R., 2014. Paleogeographic Map. http://cpgeosystems.com/paleomaps.htmlColorado Plateau Geosystems, Arizona USA.
Bodin, S., Krencker, F.-N., Kothe, T., Hoffmann, R., Mattioli, E., Heimhofer, U., Kabiri, L., 2016. Perturbation of the carbon cycle during the late Pliensbachian – early Toarcian:

New insight from high-resolution carbon isotope records in Morocco. J. Afr. Earth Sci. 116, 89–104.
Bonis, N.R., Kürschner, W.M., Krystyn, L., 2009. A detailed palynological study of the Triassic–Jurassic transition in key sections of the Eiberg Basin (Northern Calcareous Alps, Austria). Rev. Palaeobot. Palynol. 156 (3–4), 376–400.
Bougeault, C., Pellenard, P., Deconinck, J.-F., Hesselbo, S.P., Dommergues, J.-L., Bruneau, L., Cocquerez, T., Laffont, R., Huret, E., Thibault, N., 2017. Climatic and palaeoceanographic changes during the Pliensbachian (early Jurassic) inferred from clay mineralogy and stable isotope (C-O) geochemistry (NW Europe). Glob. Planet. Chang. 149, 139–152.
Bradshaw, M., Cope, J., Cripps, D., Donovan, D., Howarth, M., Rawson, P., West, I., Wimbledon, W., 1992. Atlas of palaeogeography and lithofacies. Geol. Soc. Lond 13, 107–129.
Calvert, S., Pedersen, T., 1993. Geochemistry of recent oxic and anoxic marine sediments: implications for the geological record. Mar. Geol. 113 (1–2), 67–88.
Caruthers, A.H., Smith, P.L., Gröcke, D.R., 2014. The Pliensbachian–Toarcian (early Jurassic) extinction: a north American perspective. Geol. Soc. Am. Spec. Pap. 505, 225–243.
Chadwick, R., 1986. Extension tectonics in the Wessex Basin, southern England. J. Geol. Soc. 143 (3), 465–488.
Chamley, H., 1989. Clay Formation through Weathering, Clay Sedimentology. Springer, Berlin Heidelberg, pp. 21–50.
Chandler, M.A., Rind, D., Ruedy, R., 1992. Pangaean climate during the early Jurassic: GCM simulations and the sedimentary record of paleoclimate. Geol. Soc. Am. Bull. 104 (5), 543–559.
Ciarapica, G., 2007. Regional and global changes around the Triassic–Jurassic boundary reflected in the late Norian–Hettangian history of the Apennine basins. Palaeogeogr. Palaeoclimatol. Palaeoecol. 244 (1–4), 34–51.
Clémence, M.-E., Bartolini, A., Gardin, S., Paris, G., Beaumont, V., Page, K.N., 2010. Early Hettangian benthic–planktonic coupling at Doniford (SW England). Palaeogeogr. Palaeoclimatol. Palaeoecol. 295 (1–2), 102–115.
Cohen, A.S., Coe, A.L., 2002. New geochemical evidence for the onset of volcanism in the Central Atlantic magmatic province and environmental change at the Triassic-Jurassic boundary. Geology 30 (3), 267–270.
Cohen, A.S., Coe, A.L., Bartlett, J.M., Hawkesworth, C.J., 1999. Precise Re–Os ages of organic-rich mudrocks and the Os isotope composition of Jurassic seawater. Earth Planet. Sci. Lett. 167 (3–4), 159–173.
Cohen, A.S., Coe, A.L., Harding, S.M., Schwark, L., 2004. Osmium isotope evidence for the regulation of atmospheric CO2 by continental weathering. Geology 32 (2), 157–160.
Cox, B.M., 1990. A review of Jurassic chronostratigraphy and age indicators for the UK. Geol. Soc. Lond., Spec. Publ. 55 (1), 169–190.
Črne, A.E., Weissert, H., Goričan, Š., Bernasconi, S.M., 2011. A biocalcification crisis at the Triassic-Jurassic boundary recorded in the Budva Basin (Dinarides, Montenegro). Bulletin 123 (1–2), 40–50.
Damborenea, S.E., Manceñido, M., 1979. On the palaeogeographical distribution of the pectinid genus Weyla (Bivalvia, lower Jurassic). Palaeogeogr. Palaeoclimatol. Palaeoecol. 27, 85–102.
Danisch, J., Kabiri, L., Nutz, A., Bodin, S., 2019. Chemostratigraphy of late Sinemurian–early Pliensbachian shallow-to deep-water deposits of the Central High Atlas Basin: Paleoenvironmental implications. J. Afr. Earth Sci. 153, 239–249.
Deconinck, J.-F., Hesselbo, S.P., Debuisser, N., Averbuch, O., Baudin, F., Bessa, J., 2003. Environmental controls on clay mineralogy of an early Jurassic mudrock (Blue Lias Formation, southern England). Int. J. Earth Sci. 92 (2), 255–266.
Deconinck, J.F., Hesselbo, S.P., Pellenard, P., 2019. Climatic and sea-level control of Jurassic (Pliensbachian) clay mineral sedimentation in the Cardigan Bay Basin, Llanbedr (Mochras Farm) borehole Wales. Sedimentology 66 (7), 2769–2783.
Dera, G., Donnadieu, Y., 2012. Modeling evidences for global warming, Arctic seawater freshening, and sluggish oceanic circulation during the early Toarcian anoxic event. Paleoceanography 27 (2).
Dera, G., Pucéat, E., Pellenard, P., Neige, P., Delsate, D., Joachimski, M.M., Reisberg, L., Martinez, M., 2009a. Water mass exchange and variations in seawater temperature in the NW Tethys during the early Jurassic: evidence from neodymium and oxygen isotopes of fish teeth and belemnites. Earth Planet. Sci. Lett. 286 (1–2), 198–207.
Dera, G., Pellenard, P., Neige, P., Deconinck, J.-F., Pucéat, E., Dommergues, J.-L., 2009b. Distribution of clay minerals in early Jurassic Peritethyan seas: palaeoclimatic significance inferred from multiproxy comparisons. Palaeogeogr. Palaeoclimatol. Palaeoecol. 271 (1–2), 39–51.
Dera, G., Brigaud, B., Monna, F., Laffont, R., Pucéat, E., Deconinck, J.F., Pellenard, P., Joachimski, M.M., Durlet, C., 2011. Climatic ups and downs in a disturbed Jurassic world. Geology 39 (3), 215–218.
Dera, G., Prunier, J., Smith, P.L., Haggart, J.W., Popov, E., Guzhov, A., Rogov, M., Delsate, D., Thies, D., Cuny, G., 2015. Nd isotope constraints on ocean circulation, paleoclimate, and continental drainage during the Jurassic breakup of Pangea. Gondwana Res. 27 (4), 1599–1615.
Duarte, L.V., Silva, R.F.L., Oliveira, L.V., Rengifo, M.J.C., Silva, F., 2010. Organic-Rich facies in the Sinemurian and Pliensbachian of the Lusitanian Basin, Portugal: Total organic carbon distribution and relation to transgressive-regressive facies cycles. Geol. Acta 8 (3), 325–340.
Duarte, L.V., Comas-Rengifo, M.J., Silva, R.L., Paredes, R., Goy, A., 2014. Carbon isotope stratigraphy and ammonite biochronostratigraphy across the Sinemurian-Pliensbachian boundary in the western Iberian margin. Bull. Geosci. 89, 719–736.
Emiliani, C., 1955. Pleistocene temperatures. J. Geol. 63 (6), 538–578.
Espitalié, J., Marquis, F., Barsony, I., 1984. Geochemical logging. In: Analytical Pyrolysis. Elsevier, pp. 276–304.
Espitalie, J., Deroo, G., Marquis, F., 1986. La pyrolyse Rock-Eval et ses applications. Troisième partie. Rev. Inst. Fran. Pétrole 41 (1), 73–89.
Fedo, C.M., Wayne Nesbitt, H., Young, G.M., 1995. Unraveling the effects of potassium metasomatism in sedimentary rocks and paleosols, with implications for paleoweathering conditions and provenance. Geology 23 (10).
Fleet, A., Clayton, C., Jenkyns, H., Parkinson, D., 1987. Liassic Source Rock Deposition in Western Europe, Petroleum Geology of North West Europe. Geological Society of London, London, pp. 59–70.
Föllmi, K.B., 2012. Early cretaceous life, climate and anoxia. Cretac. Res. 35, 230–257.
Föllmi, K.B., Badertscher, C., de Kaenel, E., Stille, P., John, C.M., Adatte, T., Steinmann, P., 2005. Phosphogenesis and organic-carbon preservation in the Miocene Monterey Formation at Naples Beach, California—the Monterey hypothesis revisited. GSA Bull. 117 (5–6), 589–619.
Franceschi, M., Dal Corso, J., Posenato, R., Roghi, G., Masetti, D., Jenkyns, H.C., 2014. Early Pliensbachian (early Jurassic) C-isotope perturbation and the diffusion of the Lithiotis Fauna: insights from the western Tethys. Palaeogeogr. Palaeoclimatol. Palaeoecol. 410, 255–263.
Gertsch, B., Keller, G., Adatte, T., Bartels, D., 2011. Trace-element geochemistry of Brazos sections, Texas, USA. Soc. Sedim. Geol. Spec. Publ. 100, 251–279.
Godet, A., Bodin, S., Adatte, T., Föllmi, K.B., 2008. Platform-induced clay-mineral fractionation along a northern Tethyan basin-platform transect: implications for the interpretation of early cretaceous climate change (late Hauterivian-early Aptian). Cretac. Res. 29 (5–6), 830–847.
Gómez, J.J., Comas-Rengifo, M.J., Goy, A., 2016. Palaeoclimatic oscillations in the Pliensbachian (early Jurassic) of the Asturian Basin (Northern Spain). Clim. Past 12 (5), 1199–1214.
Guex, J., Bartolini, A., Atudorei, V., Taylor, D., 2004. High-resolution ammonite and carbon isotope stratigraphy across the Triassic–Jurassic boundary at New York Canyon (Nevada). Earth Planet. Sci. Lett. 225 (1–2), 29–41.
Guex, J., Bartolini, A., Spangenberg, J., Vicente, J.-C., Schaltegger, U., 2012a. Ammonoid multi-extinction crises during the late Pliensbachian–Toarcian and carbon cycle instabilities. Solid Earth Discuss. 4 (2), 1205–1228.
Guex, J., Schoene, B., Bartolini, A., Spangenberg, J., Schaltegger, U., O'Dogherty, L., Taylor, D., Bucher, H., Atudorei, V., 2012b. Geochronological constraints on post-extinction recovery of the ammonoids and carbon cycle perturbations during the early Jurassic. Palaeogeogr. Palaeoclimatol. Palaeoecol. 346, 1–11.
Hallam, A., 1983. Early and mid-Jurassic molluscan biogeography and the establishment of the Central Atlantic seaway. Palaeogeogr. Palaeoclimatol. Palaeoecol. 43 (3–4), 181–193.
Hallam, A., 1988. A reevaluation of Jurassic eustasy in the light of new data and the revised Exxon curve. In: The Society of Economic Paleontologists and Mineralogists Special Publication. 42. pp. 261–273.
Hallam, A., 2002. How catastrophic was the end-Triassic mass extinction? Lethaia 35 (2), 147–157.
Haq, B.U., 2017. Jurassic Sea-Level Variations: a Reappraisal. Geol. Soc. Am. Today 28, 4–10.
Harazim, D., Van De Schootbrugge, B.A.S., Sorichter, K., Fiebig, J., Weug, A., Suan, G., Oschmann, W., 2013. Spatial variability of watermass conditions within the European Epicontinental Seaway during the early Jurassic (Pliensbachian-Toarcian). Sedimentology 60 (2), 359–390.
Hesselbo, S.P., 2008. Sequence stratigraphy and inferred relative sea-level change from the onshore British Jurassic. Proc. Geol. Assoc. 119 (1), 19–34.
Hesselbo, S., Jenkyns, H., 1995. A comparison of the Hettangian to Bajocian successions of Dorset and Yorkshire. Geological Society, London, pp. 105–150.
Hesselbo, S.P., Jenkyns, H.C., 1998. British lower Jurassic sequence stratigraphy. SEPM Spec. Publ. 60, 561–581.
Hesselbo, S.P., Meister, C., Gröcke, D., 2000. A potential global stratotype for the Sinemurian–Pliensbachian boundary (lower Jurassic), Robin Hood's Bay, UK: ammonite faunas and isotope stratigraphy. Geol. Mag. 137 (6), 601–607.
Hesselbo, S.P., Robinson, S.A., Surlyk, F., Piasecki, S., 2002. Terrestrial and marine extinction at the Triassic-Jurassic boundary synchronized with major carbon-cycle perturbation: a link to initiation of massive volcanism? Geology 30 (3), 251–254.
Hesselbo, S.P., Jenkyns, H.C., Duarte, L.V., Oliveira, L.C., 2007. Carbon-isotope record of the early Jurassic (Toarcian) Oceanic Anoxic Event from fossil wood and marine carbonate (Lusitanian Basin, Portugal). Earth Planet. Sci. Lett. 253 (3–4), 455–470.
Hesselbo, S.P., Hudson, A.J.L., Huggett, J.M., Leng, M.L., Riding, J.B., Ullmann, C.V., 2019. Palynological, Geochemical, and Mineralogical Characteristics of the Early Jurassic Liasidium Event in the Cleveland Basin. Newsletters on Stratigraphy, Yorkshire, UK.
Heunisch, C., Luppold, F.W., Reinhardt, L., Röhling, H.-G., 2010. Palynofazies, Bio- und Lithostratigrafie im Grenzbereich Trias/Jura in der Bohrung Mariental 1 (Lappwaldmulde, Ostniedersachsen) [Palynofacies, bio- and lithostratigraphy at the Triassic/Jurassic boundary in the Mariental 1 borehole Lappwald Syncline, Eastern Lower Saxony.]. Z. Dtsch. Ges. Geowiss. 161 (1), 51–98.
Hüsing, S.K., Beniest, A., van der Boon, A., Abels, H.A., Deenen, M.H.L., Ruhl, M., Krijgsman, W., 2014. Astronomically-calibrated magnetostratigraphy of the lower Jurassic marine successions at St. Audrie's Bay and East Quantoxhead (Hettangian–Sinemurian; Somerset, UK). Palaeogeogr. Palaeoclimatol. Palaeoecol. 403, 43–56.
Jaraula, C.M.B., Grice, K., Twitchett, R.J., Böttcher, M.E., LeMetayer, P., Dastidar, A.G., Opazo, L.F., 2013. Elevated pCO2 leading to late Triassic extinction, persistent photic zone euxinia, and rising sea levels. Geology 41 (9), 955–958.
Jenkyns, H.C., Clayton, C.J., 1986. Black shales and carbon isotopes in pelagic sediments from the Tethyan lower Jurassic. Sedimentology 33 (1), 87–106.
Jenkyns, H., Senior, J., 1991. Geological evidence for intra-Jurassic faulting in the Wessex Basin and its margins. J. Geol. Soc. 148 (2), 245–260.
Jenkyns, H.C., Weedon, G.P., 2013. Chemostratigraphy (CaCO3, TOC, δ13Corg) of

Sinemurian (lower Jurassic) black shales from the Wessex Basin, Dorset and palaeoenvironmental implications. Newsl. Stratigr. 46 (1), 1–21.
Jones, C.E., Jenkyns, H.C., Hesselbo, S.P., 1994. Strontium isotopes in early Jurassic seawater. Geochim. Cosmochim. Acta 58 (4), 1285–1301.
Kasprak, A.H., Sepúlveda, J., Price-Waldman, R., Williford, K.H., Schoepfer, S.D., Haggart, J.W., Ward, P.D., Summons, R.E., Whiteside, J.H., 2015. Episodic photic zone euxinia in the northeastern Panthalassic Ocean during the end-Triassic extinction. Geology 43 (4), 307–310.
Kent, D.V., Olsen, P.E., 2008. Early Jurassic magnetostratigraphy and paleolatitudes from the Hartford continental rift basin (eastern North America): testing for polarity bias and abrupt polar wander in association with the Central Atlantic magmatic province. J. Geophys. Res. 113 (B6).
Klug, H.P., Alexander, L.E., 1974. X-Ray Diffraction Procedures: For Polycrystalline and Amorphous Materials. John Wiley and Sons, New-York, pp. 992.
Kodina, L.A., Bogatcheva, M., Lobitzer, H., 1988. An organic geochemical study of Austrian bituminous rocks. Jahrb. Geol. Bundesanst. 131 (2), 291–300.
Korte, C., Hesselbo, S.P., 2011. Shallow marine carbon and oxygen isotope and elemental records indicate icehouse-greenhouse cycles during the early Jurassic. Paleoceanography 26 (4).
Korte, C., Hesselbo, S.P., Jenkyns, H.C., Rickaby, R.E.M., Spötl, C., 2009. Palaeoenvironmental significance of carbon- and oxygen-isotope stratigraphy of marine Triassic–Jurassic boundary sections in SW Britain. J. Geol. Soc. 166 (3), 431–445.
Kübler, B., 1983. Dosage quantitatif des minéraux majeurs des roches sédimentaires par diffraction X. Cahiers Inst. Géol. Ser. AX(1.1) 1–13.
Kuerschner, W.M., Bonis, N.R., Krystyn, L., 2007. Carbon-isotope stratigraphy and palynostratigraphy of the Triassic–Jurassic transition in the Tiefengraben section — Northern Calcareous Alps (Austria). Palaeogeogr. Palaeoclimatol. Palaeoecol. 244 (1–4), 257–280.
Kuroda, J., Hori, R.S., Suzuki, K., Gröcke, D.R., Ohkouchi, N., 2010. Marine osmium isotope record across the Triassic-Jurassic boundary from a Pacific pelagic site. Geology 38 (12), 1095–1098.
Lang, W.D., Spath, L.F., Cox, L.R., Muir-Wood, H.M., 1928. The Belemnite Marls of Charmouth, a series in the Lias of the Dorset Coast. Q. J. Geol. Soc. 84 (1–4), 179–222.
Léonide, P., Floquet, M., Villier, L., 2007. Interaction of tectonics, eustasy, climate and carbonate production on the sedimentary evolution of an early/middle Jurassic extensional basin (Southern Provence Sub-basin, SE France). Basin Res. 19 (1), 125–152.
Lu, Z., Jenkyns, H.C., Rickaby, R.E., 2010. Iodine to calcium ratios in marine carbonate as a paleo-redox proxy during oceanic anoxic events. Geology 38 (12), 1107–1110.
Luo, G., Richoz, S., van de Schootbrugge, B., Algeo, T.J., Xie, S., Ono, S., Summons, R.E., 2018. Multiple sulfur-isotopic evidence for a shallowly stratified ocean following the Triassic-Jurassic boundary mass extinction. Geochim. Cosmochim. Acta 231, 73–87.
Mander, L., Kürschner, W.M., McElwain, J.C., 2013. Palynostratigraphy and vegetation history of the Triassic–Jurassic transition in East Greenland. J. Geol. Soc. 170 (1), 37–46.
Marino, M., Santantonio, M., 2010. Understanding the geological record of carbonate platform drowning across rifted Tethyan margins: examples from the lower Jurassic of the Apennines and Sicily (Italy). Sediment. Geol. 225 (3–4), 116–137.
Marshall, J.D., 1982. Isotopic composition of displacive fibrous calcite veins; reversals in pore-water composition trends during burial diagenesis. J. Sediment. Res. 52 (2), 615–630.
McElwain, J., Beerling, D., Woodward, F., 1999. Fossil plants and global warming at the Triassic-Jurassic boundary. Science 285 (5432), 1386–1390.
McLennan, S.M., 2001. Relationships between the trace element composition of sedimentary rocks and upper continental crust. Geochem. Geophys. Geosyst. 2 (4), 1–10.
Meng, Q., Hooker, J., Cartwright, J., 2017. Early overpressuring in organic-rich shales during burial: evidence from fibrous calcite veins in the lower Jurassic Shales-with-beef member in the Wessex Basin, UK. J. Geol. Soc. 174 (5), 869–882.
Mercuzot, M., Pellenard, P., Durlet, C., Bougeault, C., Meister, C., Dommergues, J.-L., Thibault, N., Baudin, F., Mathieu, O., Bruneau, L., 2019. Carbon-Isotope Events during the Pliensbachian (Lower Jurassic) on the African and European Margins of the NW Tethyan Realm. Newsletters on Stratigraphy, PrePub Article.
Moore, D.M., Reynolds, R.C., 1989. X-Ray Diffraction and the Identification and Analysis of Clay Minerals, 322. Oxford University Press, Oxford.
Morettini, E., Santantonio, M., Bartolini, A., Cecca, F., Baumgartner, P., Hunziker, J., 2002. Carbon isotope stratigraphy and carbonate production during the Early–Middle Jurassic: examples from the Umbria–Marche–Sabina Apennines (Central Italy). Palaeogeogr. Palaeoclimatol. Palaeoecol. 184 (3–4), 251–273.
Nesbitt, H.W., Young, G., 1982. Early Proterozoic climates and plate motions inferred from major element chemistry of lutites. Nature 299 (5885), 715.
Nesbitt, H., Young, G.M., 1989. Formation and diagenesis of weathering profiles. J. Geol. 97 (2), 129–147.
Nikitenko, B.L., Mickey, M.B., 2004. Foraminifera and ostracodes across the Pliensbachian-Toarcian boundary in the Arctice Realm (stratigraphy, palaeobiogeography and biofacies). Geol. Soc. Lond. Spec. Publ. 230 (1), 137–174.
Oliveira, L., Rodrigues, R., Duarte, L.V., Lemos, V., 2006. Avaliação do potencial gerador de petróleo e interpretação paleoambiental com base em biomarcadores e isótopos estáveis do carbono da seção Pliensbaquiano-Toarciano inferior (Jurássico inferior) da região de Peniche (Bacia Lusitânica, Portugal). Boletim Geoci. Petro. 14 (2), 207–234.
Olsen, P.E., Kent, D.V., 1999. Long-period Milankovitch cycles from the late Triassic and early Jurassic of eastern North America and their implications for the calibration of the early Mesozoic time–scale and the long–term behaviour of the planets. Philos. Trans. R. Soc. Lond. 357 (1757), 1761–1786.
Olsen, P., Schlische, R., Gore, P., 1989. Field Guide to the Tectonics, Stratigraphy, Sedimentology, and Paleontology of the Newark Supergroup, Eastern North America. International Geological Congress, Guidebooks for Field Trips, pp. 174.
Olsen, P., Schlische, R., Fedosh, M., 1996. 580 ky duration of the early Jurassic flood basalt event in eastern North America estimated using Milankovitch cyclostratigraphy. Mus. North. Ariz. Bull. 60, 11–22.
Page, K.N., 2010. Stratigraphical Framework. Fossils from the Lower Lias of the Dorset Coast. Palaeontological Association, London, pp. 33–53.
Parkinson, D., 1996. Gamma-ray spectrometry as a tool for stratigraphical interpretation: examples from the western European lower Jurassic. Geol. Soc. Lond. Spec. Publ. 103 (1), 231–255.
Peti, L., Thibault, N., 2017. Abundance and size changes in the calcareous nannofossil Schizosphaerella – Relation to sea-level, the carbonate factory and palaeoenvironmental change from the Sinemurian to earliest Toarcian of the Paris Basin. Palaeogeogr. Palaeoclimatol. Palaeoecol. 485, 271–282.
Peti, L., Thibault, N., Clémence, M.-E., Korte, C., Dommergues, J.-L., Bougeault, C., Pellenard, P., Jelby, M.E., Ullmann, C.V., 2016. Sinemurian–Pliensbachian calcareous nannofossil biostratigraphy and organic carbon isotope stratigraphy in the Paris Basin: Calibration to the ammonite biozonation of NW Europe. Palaeogeogr. Palaeoclimatol. Palaeoecol. 468, 142–161.
Piper, D., Calvert, S., 2009. A marine biogeochemical perspective on black shale deposition. Earth Sci. Rev. 95 (1–2), 63–96.
Porter, S.J., Selby, D., Suzuki, K., Gröcke, D., 2013. Opening of a trans-Pangaean marine corridor during the early Jurassic: Insights from osmium isotopes across the Sinemurian–Pliensbachian GSSP, Robin Hood's Bay, UK. Palaeogeogr. Palaeoclimatol. Palaeoecol. 375, 50–58.
Price, G.D., Baker, S.J., VanDeVelde, J., Clémence, M.-E., 2016. High-resolution carbon cycle and seawater temperature evolution during the early Jurassic (Sinemurian-early Pliensbachian). Geochem. Geophys. Geosyst. 17 (10), 3917–3928.
Quan, T.M., van de Schootbrugge, B., Field, M.P., Rosenthal, Y., Falkowski, P.G., 2008a. Nitrogen isotope and trace metal analyses from the Mingolsheim core (Germany): evidence for redox variations across the Triassic-Jurassic boundary. Glob. Biogeochem. Cycles 22 (2), 1–14.
Quan, T.M., van de Schootbrugge, B., Field, M.P., Rosenthal, Y., Falkowski, P.G., 2008b. Nitrogen isotope and trace metal analyses from the Mingolsheim core (Germany): evidence for redox variations across the Triassic-Jurassic boundary. Glob. Biogeochem. Cycles 22 (2).
Quesada, S., Robles, S., Rosales, I., 2005. Depositional architecture and transgressive–regressive cycles within Liassic backstepping carbonate ramps in the Basque–Cantabrian Basin, northern Spain. J. Geol. Soc. 162 (3), 531–548.
Radley, J.D., 2008. Seafloor erosion and sea-level change: early Jurassic Blue Lias Formation of Central England. Palaeogeogr. Palaeoclimatol. Palaeoecol. 270 (3–4), 287–294.
Raymo, M., Ruddiman, W., Backman, J., Clement, B., Martinson, D., 1989. Late Pliocene variation in Northern Hemisphere ice sheets and North Atlantic deep water circulation. Paleoceanography 4 (4), 413–446.
Rees, P., Ziegler, A.M., Valdes, P.J., Huber, B., MacLeod, K., Wing, S., 2000. Jurassic Phytogeography and Climates: new Data and Model Comparisons. Warm climates in earth history, Cambridge University Press, pp. 297–318.
Richoz, S., van de Schootbrugge, B., Pross, J., Püttmann, W., Quan, T.M., Lindström, S., Heunisch, C., Fiebig, J., Maquil, R., Schouten, S., Hauzenberger, C.A., Wignall, P.B., 2012. Hydrogen sulphide poisoning of shallow seas following the end-Triassic extinction. Nat. Geosci. 5 (9), 662–667.
Riding, J.B., Leng, M.J., Kender, S., Hesselbo, S.P., Feist-Burkhardt, S., 2012. Isotopic and palynological evidence for a new early Jurassic environmental perturbation. Palaeogeogr. Palaeoclimatol. Palaeoecol. 374, 16–27.
Riediger, C.L., 2002. Hydrocarbon source rock potential and comments on correlation of the lower Jurassic Poker Chip Shale, west-Central Alberta. Bull. Can. Petrol. Geol. 50 (2), 263–276.
Rosales, I., Robles, S., Quesada, S., 2004. Elemental and oxygen isotope composition of early Jurassic belemnites: salinity vs. temperature signals. J. Sediment. Res. 74 (3), 342–354.
Rosales, I., Quesada, S., Robles, S., 2006. Geochemical arguments for identifying second-order sea-level changes in hemipelagic carbonate ramp deposits. Terra Nova 18 (4), 233–240.
Ruebsam, W., Mayer, B., Schwark, L., 2019. Cryosphere carbon dynamics control early Toarcian global warming and sea level evolution. Glob. Planet. Chang. 172, 440–453.
Ruhl, M., Kürschner, W.M., Krystyn, L., 2009. Triassic–Jurassic organic carbon isotope stratigraphy of key sections in the western Tethys realm (Austria). Earth Planet. Sci. Lett. 281 (3–4), 169–187.
Ruhl, M., Deenen, M.H.L., Abels, H.A., Bonis, N.R., Krijgsman, W., Kürschner, W.M., 2010. Astronomical constraints on the duration of the early Jurassic Hettangian stage and recovery rates following the end-Triassic mass extinction (St Audrie's Bay/East Quantoxhead, UK). Earth Planet. Sci. Lett. 295 (1–2), 262–276.
Ruhl, M., Bonis, N.R., Reichart, G.-J., Damsté, J.S.S., Kürschner, W.M., 2011. Atmospheric carbon injection linked to end-Triassic mass extinction. Science 333 (6041), 430–434.
Ruhl, M., Hesselbo, S.P., Hinnov, L., Jenkyns, H.C., Xu, W., Riding, J.B., Storm, M., Minisini, D., Ullmann, C.V., Leng, M.J., 2016. Astronomical constraints on the duration of the early Jurassic Pliensbachian Stage and global climatic fluctuations. Earth Planet. Sci. Lett. 455, 149–165.
Schaltegger, U., Guex, J., Bartolini, A., Schoene, B., Ovtcharova, M., 2008. Precise U–Pb age constraints for end-Triassic mass extinction, its correlation to volcanism and Hettangian post-extinction recovery. Earth Planet. Sci. Lett. 267 (1–2), 266–275.
Schoene, B., Guex, J., Bartolini, A., Schaltegger, U., Blackburn, T.J., 2010. Correlating the end-Triassic mass extinction and flood basalt volcanism at the 100 ka level. Geology 38 (5), 387–390.

Schöllhorn, I., Adatte, T., Charbonnier, G., Mattioli, E., Spangenberg, J.E., Föllmi, K.B., 2019. A Potential Link Between Pliensbachian Environmental Perturbations and Volcanic Activity: Swiss and British Geochemical Records.
Schwab, V., Spangenberg, J.E., Grimalt, J.O., 2006. Chemical and carbon isotopic evolution of hydrocarbons during prograde metamorphism from 100°C to 550°C: case study in the Liassic black shale formation of Central Swiss Alps. Geochim. Cosmochim. Acta 69 (7), 1825–1840.
Sell, B., Ovtcharova, M., Guex, J., Bartolini, A., Jourdan, F., Spangenberg, J.E., Vicente, J.-C., Schaltegger, U., 2014. Evaluating the temporal link between the Karoo LIP and climatic–biologic events of the Toarcian Stage with high-precision U–Pb geochronology. Earth Planet. Sci. Lett. 408, 48–56.
Sellwood, B.W., Valdes, P.J., 2008. Jurassic climates. Proc. Geol. Assoc. 119 (1), 5–17.
Shackleton, N., 1967. Oxygen isotope analyses and Pleistocene temperatures re-assessed. Nature 215 (5096), 15.
Silva, R.L., Duarte, L.V., 2015. Organic matter production and preservation in the Lusitanian Basin (Portugal) and Pliensbachian climatic hot snaps. Glob. Planet. Chang. 131, 24–34.
Silva, R., Mendonça Filho, J., Duarte, L., Comas-Rengifo, M., Azerêdo, A., Ferreira, R., 2010. Organic-rich facies of the top Ibex-Margaritatus zones (Pliensbachian) of the Lusitanian Basin (Portugal): TOC and biomarkers variation. Geochim. Cosmochim. Acta 74 (12), 962.
Silva, R.L., Duarte, L.V., Comas-Rengifo, M.J., Mendonça Filho, J.G., Azerêdo, A.C., 2011. Update of the carbon and oxygen isotopic records of the Early–late Pliensbachian (early Jurassic, ~187Ma): Insights from the organic-rich hemipelagic series of the Lusitanian Basin (Portugal). Chem. Geol. 283 (3–4), 177–184.
Smith, P.L., 1983. The Pliensbachian ammonite Dayiceras dayiceroides and early Jurassic paleogeography. Can. J. Earth Sci. 20 (1), 86–91.
Smith, D.G., 1989. Stratigraphic correlation of presumed Milankovitch cycles in the Blue Lias (Hettangian to earliest Sinemurian), England. Terra Nova 1 (5), 457–460.
Smith, P.L., Tipper, H.W., 1986. Plate tectonics and paleobiogeography: early Jurassic (Pliensbachian) endemism and diversity. Palaios 1, 399–412.
Smith, P.L., Westermann, G.E., Stanley Jr., G.D., Yancey, T.E., Newton, C.R., 1990. Paleobiogeography of the ancient Pacific. Science 249, 680–683.
Speranza, F., Parisi, G., 2007. High-resolution magnetic stratigraphy at Bosso Stirpeto (Marche, Italy): Anomalous geomagnetic field behaviour during early Pliensbachian (early Jurassic) times? Earth Planet. Sci. Lett. 256 (3–4), 344–359.
Spiro, B., 1991. Effects of minerals on rock eval pyrolysis of kerogen. J. Ther. Anal. Calorimetry 37 (7), 1513–1522.
Suan, G., Mattioli, E., Pittet, B., Mailliot, S., Lécuyer, C., 2008. Evidence for major environmental perturbation prior to and during the Toarcian (Early Jurassic) oceanic anoxic event from the Lusitanian Basin, Portugal. Paleoceanography 23 (1) (n/a-n/a).
Suan, G., Mattioli, E., Pittet, B., Lécuyer, C., Suchéras-Marx, B., Duarte, L.V., Philippe, M., Reggiani, L., Martineau, F., 2010. Secular environmental precursors to early Toarcian (Jurassic) extreme climate changes. Earth Planet. Sci. Lett. 290 (3–4), 448–458.
Suan, G., van de Schootbrugge, B., Adatte, T., Fiebig, J., Oschmann, W., 2015. Calibrating the magnitude of the Toarcian carbon cycle perturbation. Paleoceanography 30 (5), 495–509.
Surlyk, F., 2003. The Jurassic of Denmark and Greenland: the Jurassic of East Greenland: a sedimentary record of thermal subsidence, onset and culmination of rifting. Geol. Survey Denmark Greenld.Bull. 1, 659–722.
Szekely, T.S., Grose, L.T., 1972. Stratigraphy of the Carbonate, Black Shale, and Phosphate of the Pucará Group (Upper Triassic—lower Jurassic), Central Andes, Peru. Geol. Soc. Am. Bull. 83 (2), 407–428.
Them, T.R., Gill, B.C., Caruthers, A.H., Gerhardt, A.M., Gröcke, D.R., Lyons, T.W., Owens, J.D., 2018. Thallium isotopes reveal protracted anoxia during the Toarcian (Early Jurassic) associated with volcanism, carbon burial, and mass extinction. Proc. Nati. Acad. Sci. 115 (26), 20186596–20186601.
Them, T.R., Gill, B.C., Caruthers, A.H., Gröcke, D.R., Tulsky, E.T., Martindale, R.C., Smith, P.L., 2017. High-resolution carbon isotope records of the Toarcian Oceanic Anoxic Event (Early Jurassic) from North America and implications for the global drivers of the Toarcian carbon cycle. Ear. Plan. Sci. Lett. 459, 118–126.
Thiry, M., 2000. Palaeoclimatic interpretation of clay minerals in marine deposits: an outlook from the continental origin. Earth Sci. Rev. 49 (1–4), 201–221.
Tribovillard, N., Riboulleau, A., Lyons, T., Baudin, F., 2004. Enhanced trapping of molybdenum by sulfurized marine organic matter of marine origin in Mesozoic limestones and shales. Chem. Geol. 213 (4), 385–401.
Tribovillard, N., Algeo, T.J., Lyons, T., Riboulleau, A., 2006. Trace metals as paleoredox and paleoproductivity proxies: an update. Chem. Geol. 232 (1–2), 12–32.
Van Buchem, F., Melnyk, D., McCave, I., 1992. Chemical cyclicity and correlation of lower Lias mudstones using gamma ray logs, Yorkshire, UK. J. Geol. Soc. 149 (6), 991–1002.
Van de Schootbrugge, B., Bailey, T.R., Rosenthal, Y., Katz, M.E., Wright, J.D., Miller, K.G., Feist-Burkhardt, S., Falkowski, P.G., 2005. Early Jurassic climate change and the radiation of organic-walled phytoplankton in the Tethys Ocean. Paleobiology 31 (1), 73–97.
Van de Schootbrugge, B., Tremolada, F., Rosenthal, Y., Bailey, T.R., Feist-Burkhardt, S., Brinkhuis, H., Pross, J., Kent, D.V., Falkowski, P.G., 2007. End-Triassic calcification crisis and blooms of organic-walled 'disaster species'. Palaeogeogr. Palaeoclimatol. Palaeoecol. 244 (1–4), 126–141.
Van de Schootbrugge, B., Harazim, D., Sorichter, K., Oschmann, W., Fiebig, J., Püttmann, W., Peinl, M., Zanella, F., Teichert, B.M.A., Hoffmann, J., Stadnitskaia, A., Rosenthal, Y., 2010. The enigmatic ichnofossil Tisoa siphonalis and widespread authigenic seep carbonate formation during the late Pliensbachian in southern France. Biogeosciences 7 (10), 3123–3138.
Van de Schootbrugge, B., Bachan, A., Suan, G., Richoz, S., Payne, J.L., Jagt, J., 2013. Microbes, mud and methane: cause and consequence of recurrent early Jurassic anoxia following the end-Triassic mass extinction. Palaeontology 56 (4), 685–709.
Velde, B., 1995. Composition and mineralogy of clay minerals. In: Origin and Mineralogy of Clays. Springer, New-York, pp. 8–42.
Venturi, F., Bilotta, M., Ricci, C., 2006. Comparison between western Tethys and eastern Pacific ammonites: further evidence for a possible late Sinemurian–early Pliensbachian trans-Pangaean marine connection. Geol. Mag. 143 (5), 699–711.
Venturi, F., Nannarone, C., Bilotta, M., 2007. Ammonites from the early Pliensbachian of the Furlo Pass (Marche, Italy): biostratigraphic and paleobiogeographic implications. Boll. Soc. Paleontol. Ital. 46 (1), 1.
Ward, P.D., Garrison, G.H., Williford, K.H., Kring, D.A., Goodwin, D., Beattie, M.J., McRoberts, C.A., 2006. The organic carbon isotopic and paleontological record across the Triassic–Jurassic boundary at the candidate GSSP section at Ferguson Hill, Muller Canyon, Nevada, USA. Palaeogeogr. Palaeoclimatol. Palaeoecol. 244 (1–4), 281–289.
Warrington, G., Ivimey-Cook, H.C., 1995. The late Triassic and early Jurassic of coastal sections in West Somerset and South and Mid-Glamorgan. Gol. Soc. Lond. 9–30.
Wedepohl, K., 1971. Environmental influences on the chemical composition of shales and clays. Phys. Chem. Earth 8, 307–333.
Wedepohl, K., 1991. Chemical composition and fractionation of the continental crust. Geol. Rundsch. 80 (2), 207–223.
Weedon, G., 1986. Hemipelagic shelf sedimentation and climatic cycles: the basal Jurassic (Blue Lias) of South Britain. Earth Planet. Sci. Lett. 76 (3–4), 321–335.
Weedon, G., Jenkyns, H., 1999. Cyclostratigraphy and the early Jurassic timescale: data from the Belemnite Marls, Dorset, southern England. Geol. Soc. Am. Bull. 111 (12), 1823–1840.
Weedon, G.P., Jenkyns, H.C., Page, K.N., 2017. Combined sea-level and climate controls on limestone formation, hiatuses and ammonite preservation in the Blue Lias Formation, South Britain (uppermost Triassic – lower Jurassic). Geol. Mag. 155 (05), 1117–1149.
Weedon, G.P., Page, K.N., Jenkyns, H.C., 2018. Cyclostratigraphy, stratigraphic gaps and the duration of the Hettangian Stage (Jurassic): insights from the Blue Lias Formation of southern Britain. Geol. Mag. 1–41.
Wignall, P., 2001. Sedimentology of the Triassic–Jurassic boundary beds in Pinhay Bay (Devon, SW England). Proc. Geol. Assoc. 112 (4), 349–360.
Williford, K.H., Ward, P.D., Garrison, G.H., Buick, R., 2007. An extended organic carbon-isotope record across the Triassic–Jurassic boundary in the Queen Charlotte Islands, British Columbia, Canada. Palaeogeogr. Palaeoclimatol. Palaeoecol. 244 (1–4), 290–296.
Woodfine, R.G., Jenkyns, H.C., Sarti, M., Baroncini, F., Violante, C., 2008. The response of two Tethyan carbonate platforms to the early Toarcian (Jurassic) oceanic anoxic event: environmental change and differential subsidence. Sedimentology 55 (4), 1011–1028.
Xu, W., Ruhl, M., Hesselbo, S.P., Riding, J.B., Jenkyns, H.C., 2016. Orbital pacing of the early Jurassic carbon cycle, black-shale formation and seabed methane seepage. Sedimentology 64 (1), 127–149.
Yager, J.A., West, A.J., Corsetti, F.A., Berelson, W.M., Rollins, N.E., Rosas, S., Bottjer, D.J., 2017. Duration of and decoupling between carbon isotope excursions during the end-Triassic mass extinction and Central Atlantic Magmatic Province emplacement. Earth Planet. Sci. Lett. 473, 227–236.
Yan, D., Chen, D., Wang, Q., Wang, J., 2010. Large-scale climatic fluctuations in the latest Ordovician on the Yangtze block, South China. Geology 38 (7), 599–602.
Zachos, J., Pagani, M., Sloan, L., Thomas, E., Billups, K., 2001. Trends, rhythms, and aberrations in global climate 65 Ma to present. Science 292 (5517), 686–693.
Ziegler, P., 1990. Geological Atlas of Western and Central Europe. 2. Shell Internationale Petroleum Maatschappij BV and Geological Society of London, pp. 239.